FEATURE ARTICLE

Ab Initio Calculations of Vibronic Spectra and Dynamics for Small Polyatomic Molecules: Role of Duschinsky Effect

A. M. Mebel,[†] M. Hayashi,[†] K. K. Liang,[†] and S. H. Lin*[,†,‡,§]

Institute of Atomic and Molecular Sciences, Academia Sinica, P.O. Box 23-166, Taipei 10764, Taiwan, ROC, Department of Chemistry and Biochemistry, Arizona State University, Tempe, Arizona 85284-1604, and Department of Chemistry, National Taiwan University, Taipei, Taiwan, ROC

Received: July 15, 1999; In Final Form: September 24, 1999

The Duschinsky effect has been shown to be significant in spectroscopy and dynamics of molecules that involve the $\pi-\pi^*$ transitions. In this paper, we present a derivation of exact expressions for optical absorption and radiationless transitions in polyatomic molecules with displaced−distorted−rotated harmonic potential surfaces. In the formulation, we take into account the temperature effect exactly. The application of this new formulation is demonstrated for ethylene and allene, where the Duschinsky effect in the first singlet excited electronic state is very strong.

I. Introduction

Ab initio molecular orbital (MO) calculations of potential energy surfaces (PES) for excited electronic states are increasingly becoming a powerful tool in studies of molecular spectroscopy and photochemistry.[1] Accurate calculation of the excited-state surfaces is a complex task that requires the use of advanced ab initio methods such as the multiconfigurational complete active space SCF (CASSCF)[2] or the equation-of-motion coupled cluster (EOM-CCSD)[3] methods for geometry optimization and vibrational frequency calculations and the multireference configuration interaction (MRCI) method[4] or multiconfigurational perturbation theory (CASPT*n*, CASMP*n*)[5] for refinement of energies. Most theoretical studies of excited electronic states reported in the literature consider only vertical excitation energies in the Franck−Condon region. However, behavior of excited states beyond this region is relevant to the spectroscopy and dynamics of photochemical reactions.

An ab initio approach for the calculations of vibronic spectra for polyatomic molecules includes accurate calculations of potential energy surfaces for the ground and excited states, which provide the information about vertical and adiabatic excitation energies, oscillator strengths for various transitions, equilibrium geometries, vibrational frequencies, and normal coordinates for the ground and excited states, transition matrix elements, etc. Such information allows us to compute the positions and intensities (Franck−Condon factors) of various peaks in vibronic spectra using the harmonic approximation for nuclear motion. A common feature of most spectral intensity calculations for polyatomic molecules is the use of ad hoc model potentials that include one or two degrees of freedom. A more general approach would be to compute the Franck−Condon factors from first principles, i.e., from the potential energy surfaces of the ground and excited states obtained by ab initio MO calculations. The complexity of such an approach owes itself to the fact that in an excited state the normal modes can often be not only displaced and distorted but also mixed with each other, which makes the calculations of the vibrational overlap integrals between the ground and excited-state normal coordinates nontrivial. Here, normal mode displacement means a geometry change from the ground to excited state, i.e., displacement of the position of a local minimum on the potential energy surface, distortion corresponds to a change of vibrational frequencies reflecting a change of the surface shape, and normal mode mixing or rotation is alteration of the character of normal modes after electronic excitation.

The mode mixing in the excited electronic state with respect to the ground state was first described[6] by a Russian scientist in 1937 and is generally called the Duschinsky effect. This phenomenon is recognized as one of the main reasons for dissymmetry between absorption and emission spectra. It is also responsible for the appearance in the spectra of combined transitions due to normal modes *X* and *Y* where only mode *X* is optically active and *Y* is mixed with *X* in the excited state. In general, the Duschinsky effect scrambles the occupation of the normal modes, leading to unusual intensity distributions. The phenomenon of mode mixing has been observed in the absorption and emission spectra of many organic molecules such as benzene,[7] naphthalene,[8] α- and β-methylnaphthalenes,[9] phenanthrene,[8] pyridine,[10] azulene and azaazulenes,[11−13] styrene,[14] benzyl radical,[15] *N*,*N*′-dicyanoquinodiimines,[16] 1,3,5-tri-*tert*-butylpentalene,[17] 2-phenylindole,[18] *o*-difluorobenzene,[19] ethynylbenzene (phenylacetylene),[20,21] tetracyanoquinodimethane anion ($TCNQ^-$) and naphthalene cation,[22] anthracene,[23] blue copper proteins,[24] etc. For symmetry-allowed electronic transitions, the Duschinsky effect can be studied from the different intensity distributions displayed in absorption and emission and from the presence of combination bands revealed by single vibronic level excitation spectroscopy. For example,[25] the single level fluorescence (SVLF) spectra of *cis*-2-methoxynaphthalene reveal strong vibrational mixing in the S_1 state and could be assigned on the basis of the Duschinsky rotation. In molecules with a symmetry-forbidden electronic transition, such as benzene,[7] the amount of mode rotation in this state can be detected by examining the two-photon excitation spectra of several deuterated isotopomers.

[†] Academia Sinica.
[‡] Arizona State University.
[§] National Taiwan University.

10.1021/jp992429m CCC: $18.00
Published on Web 12/16/1999

The Duschinsky effect can play a role not only in the absorption, emission, and fluorescence spectra but also in the resonance Raman spectra[26−28] (influence on the nonlinear optical susceptibilities and coherent line shapes in large molecules) and sum frequency generation (SFG) spectra from adsorbed molecules.[29] The mode mixing can affect the rates of internal conversion between different electronic states through alteration of the Franck−Condon factor (vibrational part of the rate constant).[1,30,31] The structural and dynamical consequences of the rotational Duschinsky effect on rotationally resolved fluorescence excitation spectra have been also reported.[32]

A classical example of the Duschinsky effect is found in interpretation of the absorption spectra for *cis*- and *trans*-hexatriene.[33,34] Although the two isomers are very similar, their ultraviolet absorption spectra corresponding to the $^1B_1 \leftarrow {}^1A_1$ and $^1B_u \leftarrow {}^1A_g$ transitions to the S_2 state are markedly different. For instance, the intensity of the first intense band is lower for *cis*-hexatriene than for the *trans*-hexatriene; the intensity of subsequent vibronic peaks is redistributed in the direction of larger energies, indicating a larger distortion of the cis isomer after electronic excitation. The total width of the cis isomer spectrum is larger, the peaks are markedly broader, and several shoulders are much more marked in the cis hexatriene spectrum. Petelenz and Petelenz[35] first gave a theoretical explanation of this phenomenon based on the Duschinsky effect. They considered a simple model taking into account three normal modes corresponding to a double CC bond stretching motion, a single CC bond stretching mode, and a central bond bending mode. They wrote model vibrational Hamiltonians for the ground and excited states of the trans and cis isomers. Because of a steric hindrance in *cis*-hexatriene, the normal modes are mixed in the excited state of this isomer. This results in intensity redistribution of vibronic peaks and the broader and more complicated character of the absorption spectrum for *cis*-hexatriene compared to that for *trans*-hexatriene. Hemley et al.[36] carried out a theoretical analysis of the absorption spectra for the two isomers using the semiempirical extended PPP-CI approach. They analyzed in detail for both isomers the vibrational structure in the excited state, including frequency shifts from the ground state and Duschinsky mixing. Indeed, the mixing appeared to be heavier in the *cis*-structure than in the *trans*-hexatriene. Hemley et al.[36] have also concluded that the differences in the spectra are related to the differences in the excited-state geometries: planar configuration for trans and a geometry that is slightly twisted about the central bond for cis. Zerbetto and Zgiersky[37] returned to the analysis of the spectra for *cis*- and *trans*-hexatriene using the ab initio CIS method. The Duschinsky rotational matrices computed at this level are in qualitative agreement with the findings of Hemley et al.,[36] although ab initio values tend to provide a picture of more drastic rotations. In general, ab initio calculations give the calculated spectra in satisfactory agreement with experimental absorption spectra of the two isomers of hexatriene.

The calculations of vibronic peak intensities taking into account the Duschinsky effect require computations of multidimensional vibrational overlap integrals, which are of formidable analytical complexity and cannot be represented as simple products of one-dimensional integrals. One of the first attempts of a quantitative analysis of this problem was made by Coon, DeWames, and Loyd[38] who suggested an approximate method for calculating two-dimensional integrals specifically for nonlinear triatomic systems. Atabek, Bourgeois, and Jacon computed Franck−Condon factors taking into account two-mode mixing for a special case of symmetric triatomic molecules, ABA.[39] The calculations were applied to the studies of isotope effects in the photofragmentation of triatomic molecules where the initial vibrational energy content was related to the dissociation cross sections and branching ratios measuring the competition between different isotope fragmentation arrangements. The same approach was applied to the study of the absorption and fluorescence spectra of ozone[40] where the Duschinsky effect originates from the coupling of bending and stretching motions in the excited state. Recently, Smith[41] analyzed the effect of strong Duschinsky mixing of two normal coordinates Q_1 and Q_2 on the intensity in nontotally symmetric vibrations in electronic spectra. He used a Fermi resonance type theory and derived the expressions for the intensity of transitions such as $1_0^1 2_1^0$ and $1_0^1 2_0^1$, which gain significant intensity when mixing of coordinates is strong. The results were applied to the electronic spectra of styrene, tropolone, and 1,4-benzodioxan, which provide examples of strong mixing between a pair of normal coordinates.

Sharp and Rosenstock[42] as well as Smith and Warsop[43] developed a more general approach in which a generating function was derived and the Franck−Condon integrals are obtained as coefficients in the expansion of this function in a multiple-power series of dummy variables. In this way they were able to determine relative probabilities of transitions starting from the vibrationless level of the ground electronic state to overtones and to some low combination levels of an excited electronic state. The method of Sharp and Rosenstock is a direct expansion of the method used by Hutchisson[44] for the one-dimensional case, and it provides an expression from which one can evaluate the individual Franck−Condon factors by a finite series expansion. The generating function technique was also used by Karplus and Warshal[45,46] to study vibronic spectra of conjugated hydrocarbons. The coherent-state method of Doktorov et al.[47,48] gave the same expressions as the method of Sharp and Rosenstock;[42] however, they additionally provided some recurrence relations for the two- and multidimensional Franck−Condon integrals. The coefficients in these recurrence equations were given explicitly for $N = 2$ only. Doktorov et al. applied their method to analyzing the intensity distribution of single mode progressions in the $^1B_{2u} \leftarrow {}^1A_{1g}$ electronic transition in benzene. Kupka and Cribb[49] continued the development of the generating function method and derived the multidimensional integrals by means of a multivariable generating function that incorporates both the transformation of the normal coordinates between two electronic states and their frequency changes. With the help of this generating function, $2N$ recurrence equations (i.e., one recurrence equation for each of the excited and ground state occupation numbers) were derived. The solution of these equations for three vibrational degrees of freedom was given and applied to resonance Raman scattering. The results demonstrated that the corresponding cross section is strongly affected by mode mixing.

Another approach to compute polyatomic Franck−Condon integrals has been suggested by Faulkner and Richardson.[50] They used contact transformation perturbation theory to construct the vibrational wave functions of an excited state in terms of the vibrational wave functions of the ground state. Then the calculation of multidimensional vibrational overlap integrals is reduced to the evaluation of vibrational matrix elements exclusively within the ground-state vibrational manifold. However, this method is unsuccessful because of the slow convergence of the perturbation expansion.[50,51] Another method developed by the same authors[50] used a linear transformation of the normal coordinates to remove the Duschinsky rotation. The multidimensional Franck−Condon integrals are then expressed as sums of factorizable integrals in the new intermediate

nuclear coordinates. This method has better computational efficiency than the perturbation method but is restricted to the zero-temperature limit. Özkan[52] has employed the operator technique to calculate matrix elements between shifted and distorted harmonic oscillator functions (which can be associated with one or two distinct electronic states) and derived some recurrence relations for one, two, and three oscillators. More recently, Chen et al.[53] have transformed the two-dimensional Franck−Condon integrals into a separable form, but the resulting expression contains infinite expansions over the associated Laguerre polynomials, and integration over the normal coordinates remains unevaluated. A new approximate method for indirect calculations of the superposition integrals of the vibrational wave functions of the combined electronic states based on the variational solution of the vibrational problem in the excited state was proposed in 1995 by Baranov and Zelentsov.[54]

Most of the practical applications to the studies of vibronic spectra for polyatomic molecules taking into account the Duschinsky effect are based on the semiempirical or molecular mechanics calculations of the normal coordinates in the ground and excited electronic states and on the method of Sharp and Rosenstock[42] to compute the Franck−Condon factors. For instance, Hemley et al.[14] carried out theoretical vibrational analysis of the UV spectrum of styrene using the extended PPP-CI method, which computes the ground and lowest excited singlet states of this molecule. As mentioned above, the same group used a similar approach to study the vibronic spectra of *cis*- and *trans*-hexatriene.[36] Zerbetto and Zgiersky are particularly active in this field; they employed the QCFF-PI and CNDO/S+CISD method to investigate the spectroscopic behavior of various polyenes such as anthracene, nystatin, and butadiene.[55−57] More recent applications based on semiempirical potential energy surfaces include the calculation of the Duschinsky effect in phenol by Venuti and Marconi[58] and the study of 1,3,5-tri-*tert*-butylpentalene by Falchi et al.[17] Studies based on ab initio potential energy surfaces have appeared only recently and are still rare. Chau et al.[59] studied the vibrational structure of the He I photoelectron spectrum of H_2Se based on the high-level CCSD(T) geometry optimization and harmonic vibrational frequency computation and used Chen's method[60] to compute the Franck−Condon factors. Crane et al.[61] carried out the vibrational assignment of the S_1 fluorescence excitation spectrum of formyl fluoride also using high-level ab initio potential energy surfaces. The Franck−Condon factors were calculated with account of the Duschinsky rotation using the computer program of Chen,[62] which implements the method of Sharp and Rosenstock.[42]

Recently,[63,64] we derived a closed-form expression for the four-dimensional vibrational overlap integral that is evaluated in terms of products of Hermite polynomials. The expression is valid for the case of the vibrationless ground electronic state and takes into account distortion, displacement, and normal mode mixing (up to four modes). We applied this approach to compute the $\pi-\pi^*$ vibronic spectrum of ethylene based on the ab initio potential energy surfaces for this molecule in the ground ^1A_g and excited $^1B_{1u}$ electronic states. The geometry of C_2H_4 changes significantly in the $\pi-\pi^*$ state by twisting the CH_2 groups by 90°. This leads to heavy mixing of four normal modes of "a" symmetry within the D_2 point group common for the ground (D_{2h}) and excited (D_{2d}) state geometries. The ab initio calculations of Franck−Condon factors taking into account the Duschinsky effect allowed us to interpret major features of the experimental spectrum of ethylene and showed that the $\pi-\pi^*$ transition is responsible for the broad continuous distribution between 5.6 and 11 eV (underlying continuum). The role of Duschinsky mixing is crucial; it makes the spectrum broad and dense.

We used a similar ab initio approach to calculate vibronic spectra of various polyatomic molecules and radicals such as CH_4,[65] CH_3,[66] C_2H_3,[67] C_3H_2,[68,69] and $(CH_3)_2CO$.[70] Our studies show that the normal mode rotation is significant in methane and vinyl radical. All nine normal coordinates are mixed in the $S_1 \leftarrow S_0$ electronic transition of CH_4, and the absorption spectrum consists of a broad and almost featureless band between 8.3 and 11.3 eV.[65] In the $1^2A'' \leftarrow 1^2A'$ transition of the vinyl radical the mode mixing is not so heavy and the vibronic spectrum reveals distinct features.[67] The Duschinsky effect leads to a redistribution of intensities for various vibronic peaks. For all the molecules we studied, the ab initio calculated vibronic spectra are in good agreement with experimental data.

The normal mode rotation also plays a role in radiationless transitions between different electronic states, since the expressions for the rate constants of internal conversion (IC) and intersystem crossing (ISC) contain a vibrational part (Franck−Condon factor).[71−74] We considered[30] the case when several accepting normal modes are mixed with each other and derived explicit expressions for the IC rates, taking into account the displacements, distortions of normal modes, and the Duschinsky effect for the case of the vibrationless initial electronic state ($T = 0$). We demonstrated the effect of rotated normal modes on the IC rate constants on the basis of a model consisting of one promoting and two mixed accepting modes. The technique was applied to calculate the rate of internal conversion between the excited singlet $\pi-\pi^*$ and ground electronic states in ethylene.[30]

In combination with accurate ab initio potential energy surfaces, precise calculations of Franck−Condon factors for the general case of displaced, distorted, and rotated normal modes and nonzero temperature would be an invaluable tool for theoretical studies of vibronic spectra, electronic relaxation, and photodissociation dynamics. Recently,[75] in this group a new closed-form expression for the Franck−Condon integrals for overlap between arbitrary multidimensional harmonic oscillators was exactly derived. Some simple rules were deduced whereby an arbitrary multidimensional Franck−Condon integral $\langle \nu_1 ... \nu_N | \nu_1' ... \nu_N' \rangle$ can be expressed as a sum of products of Hermite polynomials.

In this article, we present a derivation of exact expressions for optical absorption and radiationless transitions in polyatomic molecules with displaced−distorted−rotated harmonic potential surfaces. The application of this new theory is demonstrated for ethylene, where the Duschinsky effect in the first singlet excited electronic state is very strong. It can be expected that the Duschinsky effect would be very significant for the $\pi-\pi^*$ transitions of polyatomic molecules. It should be emphasized that the calculations of absorption spectra and radiationless transitions are based on the potential surfaces obtained from ab initio calculations.

II. Theory

Spectroscopy. The absorption coefficient for the electronic transition a → b in the Condon approximation can be expressed as

$$\alpha(\omega) = \frac{4\pi^2\omega}{3\hbar c}|\vec{\mu}_{ba}|^2 \sum_{v}\sum_{v'} P_{av}|\langle \Theta_{bv'}|\Theta_{av}\rangle|^2\, \delta(\omega_{bv',av}-\omega) \quad (1)$$

which can be rewritten as

$$\alpha(\omega) = \frac{2\pi\omega}{3\hbar c}|\vec{\mu}_{ba}|^2 \int_{-\infty}^{\infty} dt\, e^{it(\omega_{ba}-\omega)}\, G(t) \quad (2)$$

Here, $G(t)$ denotes the correlation function and is given by

$$G(t) = \sum_{v}\sum_{v'} P_{av}|\langle\Theta_{bv'}|\Theta_{av}\rangle|^2 \exp\left[\frac{it}{\hbar}(E_{bv'} - E_{av})\right] \quad (3)$$

Let us consider the general case; that is, a molecular system consists of N_d modes exhibiting the Duschinsky effect and N modes without mode-mixing. In this case, $G(t)$ can be written as

$$G(t) = G_{12\ldots N_d}(t) \prod_{l}^{l\neq 1,2\ldots N_d} G_l(t) \quad (4)$$

where $G_{12\ldots N_d}(t)$ and $G_l(t)$ denote the correlation functions defined by

$$G_l(t) = \sum_{v_l}\sum_{v_l'} P_{av_l}|\langle\chi_{bv_l'}(Q_l')|\chi_{av_l}(Q_l)\rangle|^2 \exp\left[it\left\{\left(v_l' + \frac{1}{2}\right)\omega_l' - \left(v_l + \frac{1}{2}\right)\omega_l\right\}\right] \quad (5)$$

and

$$G_{12\ldots N_d}(t) = \sum_{v_1}\cdots\sum_{v_{N_d}}\sum_{v_{\alpha_1}'}\cdots\sum_{v_{\alpha_{Nd}}'} P_{av_1\ldots v_{Nd}}|\langle\chi_{bv_{\alpha 1}'}(Q_{\alpha_1}')\cdots\chi_{bv_{\alpha Nd}'}(Q_{\alpha_{Nd}}') \times |\chi_{av_1}(Q_1)\cdots\chi_{av_{Nd}}(Q_{N_d})\rangle|^2 \exp\left[it\left\{\sum_{\alpha=\alpha_1}^{\alpha_{N_d}}\left(v_\alpha' + \frac{1}{2}\right)\omega_\alpha' - \sum_{j=1}^{N_d}\left(v_j + \frac{1}{2}\right)\omega_j\right\}\right] \quad (6)$$

That is, $G_{12\ldots N_d}(t)$ represents the correlation function of the mixing modes (i.e., the Duschinsky effect).

Making use of the Slater sum (see eq A4 in Appendix A), we obtain

$$G_{12\cdots N_d}(t) = \prod_{j=1}^{N_d}\left\{\frac{2\sqrt{\beta_j}\sinh\frac{\hbar\omega_j}{2kT}}{\sqrt{2\pi\sinh\lambda_j}}\right\}\prod_{\alpha=\alpha_1}^{\alpha_{N_d}}\left\{\frac{\sqrt{\beta_\alpha'}}{2\pi\sinh\mu_\alpha'}\right\} \times \prod_{j=1}^{N_d}\{\int_{-\infty}^{\infty} dQ_j \int_{-\infty}^{\infty} d\bar{Q}_j\} \exp\left[-\sum_{j=1}^{N_d}\frac{\beta_j}{4}\left\{(Q_j + \bar{Q}_j)^2 \tanh\frac{\lambda_j}{2} + (Q_j - \bar{Q}_j)^2 \coth\frac{\lambda_j}{2}\right\}\right] \exp\left[-\sum_{\alpha=\alpha_1}^{\alpha_{N_d}}\frac{\beta_\alpha'}{4}\left\{(Q_\alpha' + \bar{Q}_\alpha')^2 \tanh\frac{\mu_\alpha'}{2} + (Q_\alpha' - \bar{Q}_\alpha')^2 \coth\frac{\mu_\alpha'}{2}\right\}\right] \quad (7)$$

where $\beta_j = \omega_j/\hbar$, $\beta_\alpha = \omega_\alpha'/\hbar$, $\lambda_j = i\omega_j + \hbar\omega_j/(kT)$, $\mu_\alpha = -i\omega_\alpha'$, and

$$Q_\alpha' = \sum_{j=1}^{N_d} C_{\alpha j}(Q_j + \Delta Q_j) \quad (8)$$

for $\alpha = \alpha_1, \ldots, \alpha_{N_d}$. It follows that

$$G_{12\cdots N_d}(t) = e^{-D}\prod_{j=1}^{N_d}\left\{\frac{2\sqrt{\beta_j}\sinh\frac{\hbar\omega_i}{2kT}}{\sqrt{2\pi\sinh\lambda_i}}\right\} \times \prod_{\alpha=\alpha_1}^{\alpha_{N_d}}\left\{\frac{\sqrt{\beta_\alpha'}}{\sqrt{2\pi\sinh\mu_\alpha'}}\right\}\prod_{j=1}^{N_d}\{\int_{-\infty}^{\infty} dQ_j \int_{-\infty}^{\infty} d\bar{Q}_j\} \times \exp[-\sum_{j=1}^{N_d}A_{jj}(Q_j + \bar{Q}_j)^2 - \sum_{j=1}^{N_d}\sum_{k>j}^{N_d}A_{jk}(Q_j + \bar{Q}_j)(Q_k + \bar{Q}_k)] \times \exp[-\sum_{j=1}^{N_d}A_j(Q_j + \bar{Q}_j)] \exp[-\sum_{j=1}^{N_d}B_{jj}(Q_j - \bar{Q}_j)^2 - \sum_{j=1}^{N_d}\sum_{k>j}^{N_d}B_{jk}(Q_j - \bar{Q}_j)(Q_k - \bar{Q}_k)] \quad (9)$$

where

$$A_{jj} = \frac{\beta_j}{4}\tanh\frac{\lambda_j}{2} + \sum_{\alpha=\alpha_1}^{\alpha_{N_d}}\frac{\beta_\alpha'}{4}\tanh\frac{\mu_\alpha'}{2}(C_{aj})^2 \quad (10)$$

$$A_{jk} = \sum_{\alpha=\alpha_1}^{\alpha_{N_d}}\frac{\beta_\alpha'}{2}\tanh\frac{\mu_\alpha'}{2}C_{\alpha j}C_{\alpha k} \quad (11)$$

$$A_j = \sum_{\alpha=\alpha_1}^{\alpha_{N_d}}\sum_{k=1}^{N_d}\beta_\alpha'\tanh\frac{\mu_\alpha'}{2}C_{\alpha j}C_{\alpha k}\Delta Q_k \quad (12)$$

$$B_{jj} = \frac{\beta_j}{4}\coth\frac{\lambda_j}{2} + \sum_{\alpha=\alpha_1}^{\alpha_{N_d}}\frac{\beta_\alpha'}{4}\coth\frac{\mu_\alpha'}{2}(C_{\alpha j})^2 \quad (13)$$

$$B_{jk} = \sum_{\alpha=\alpha_1}^{\alpha_{N_d}}\frac{\beta_\alpha'}{2}\coth\frac{\mu_\alpha'}{2}C_{\alpha j}C_{\alpha k} \quad (14)$$

and

$$D = \sum_{\alpha=\alpha_1}^{\alpha_{N_d}}\beta_\alpha'\tanh\frac{\mu_\alpha'}{2}(\sum_{j=1}^{N_d}C_{\alpha j}\Delta Q_j)^2 \quad (15)$$

Some of the particular cases are given in Appendix A.

Next we shall calculate $G_i(t)$ given by eq 5 for the displaced and distorted harmonic oscillator case. It is given by

$$G_l(t) = \frac{2\beta_l\beta_l'\sinh\frac{\hbar\omega_l}{2kT}}{\sqrt{\left(\beta_l\tanh\frac{\lambda_l}{2} + \beta_l'\tanh\frac{\mu_l'}{2}\right)\left(\beta_l\coth\frac{\lambda_l}{2} + \beta_l'\coth\frac{\mu_l'}{2}\right)}} \times \exp\left[-\frac{\beta_l\beta_l'\Delta Q_l^2}{\beta_l\coth\frac{\mu_l'}{2} + \beta_l'\coth\frac{\lambda_l}{2}}\right] \quad (16)$$

Dynamics. The rate of internal conversion (IC) for the electronic transition b → a in the Condon approximation can be expressed as[72]

$$W = \frac{2\pi}{\hbar}|R_p(ba)|^2\sum_{v}\sum_{v'}P_{bv'}|\left\langle\Theta_{bv'}\left|\frac{\partial}{\partial Q_p}\right|\Theta_{av}\right\rangle|^2\,\delta(E_{bv'} - E_{av}) \quad (17)$$

where

$$R_p(ba) = -\hbar^2\left\langle \Phi_b \left| \frac{\partial}{\partial Q_p} \right| \Phi_a \right\rangle \tag{18}$$

Here, for simplicity it is assumed that only one promoting mode Q_p is responsible for IC. Note that

$$W = \frac{1}{\hbar^2}|R_p(ba)|^2 \int_{-\infty}^{\infty} dt\, e^{it\omega_{ba}} K_p(t)\, \bar{G}(t) \tag{19}$$

where

$$K_p(t) = \sum_{v}\sum_{v'} P_{bv'_p}\left|\left\langle \chi_{bv'_p}(Q'_p)\left|\frac{\partial}{\partial Q_p}\right|\chi_{av_p}(Q_p)\right\rangle\right|^2 \exp\left[it\left\{\left(v_p + \frac{1}{2}\right)\omega_p - \left(v'_p + \frac{1}{2}\right)\omega'_p\right\}\right] \tag{20}$$

Here, $\bar{G}(t)$ in eq 19 is equivalent to $G(t)$ without the promoting mode contribution. The other difference between $\bar{G}(t)$ and $G(t)$ is that the initial and final vibronic states should be reversed.

It should be noted that $K_p(t)$ can be expressed as

$$K_p(t) = \frac{1}{2}G_p(t)\left[\frac{\beta'_p\beta_p}{\beta_p \tanh\frac{\lambda'_p}{2} + \beta'_p \tanh\frac{\mu_p}{2}} - \frac{\beta'_p\beta_p}{\beta_p \coth\frac{\lambda'_p}{2} + \beta'_p \coth\frac{\mu_p}{2}} + \frac{2\beta'^2_p\beta^2_p(\Delta Q_p)^2}{\left(\beta'_p \coth\frac{\lambda_p}{2} + \beta_p \coth\frac{\mu'_p}{2}\right)^2}\right] \tag{21}$$

where $G_p(t)$ is given by exchanging λ_l, μ'_l, β_l, and β'_lin eq 16 with λ'_p, μ_p, β'_p, and β_p, respectively.

III. Applications

A. Model System. In the previous section, we have derived an expression for the absorption spectra of a molecular system consisting of N_d modes exhibiting the Duschinsky effect. It is instructive to investigate the role of mode mixing for a model system with two mixing modes. We set a model for the Duschinsky matrix elements,

$$\begin{pmatrix} Q_{a1} \\ Q_{a2} \end{pmatrix} = \begin{pmatrix} \cos\varphi & \sin\varphi \\ -\sin\varphi & \cos\varphi \end{pmatrix}\begin{pmatrix} Q_1 + \Delta Q_1 \\ Q_2 + \Delta Q_2 \end{pmatrix} \tag{22}$$

By using the fast Fourier transform algorithm for numerical calculation, we can study the Duschinsky effect and temperature effect on the two-mode mixing system.

Figure 1 shows the effect of mode mixing on the absorption spectra of a distorted and rotated system. The right and left panels show the calculated absorption spectra at 0 and 500 K, respectively. In each panel, the top, middle, and bottom panels demonstrate the absorption spectra as a function of φ. For these calculations, we use several parameters: $\hbar\omega_1 = 3001$ cm^{-1}, $\hbar\omega_2 = 850$ cm^{-1}, $\hbar\omega_{a1} = 3027$ cm^{-1}, $\hbar\omega_{a2} = 977$ cm^{-1}, $\Delta Q_1 = \Delta Q_2 = 0$ Å amu$^{1/2}$. For simplicity, we translate the 0−0 transition energy to 5000 cm^{-1}. We use the fast Fourier transform algorithm with 262 144 points to generate the correlation function eq 4. The frequency resolution is set to be 2 cm^{-1}, and we employ 2 cm^{-1} as a convergence factor. This factor does not influence the results, since its value is only 0.26% of the lowest vibrational frequency of this system.

One can see from Figure 1 that the absorption spectra do not depend on the sign of φ in the case in which the system has only distorted and rotated harmonic potential surfaces. This feature can easily be seen from eqs B3, B4, B6, and B7. We find that the signs of Duschinsky matrix elements depend only on eq B4. In the case of $\Delta Q_1 = \Delta Q_2 = 0$, eq B4 becomes 0 so that no sign dependence can be observed.

The absorption spectra will exhibit a strong sign dependence in the case in which $\Delta Q_1 \neq 0$ and $Q_2 \neq 0$, that is, once the potential is displaced. Figure 2 demonstrates the absorption spectra of a system consisting of displaced−distorted−rotated harmonic potentials. For these calculations, we use the same parameters except for the displacements: $\Delta Q_1 = 0.449$ Å amu$^{1/2}$ and $\Delta Q_2 = 1.321$ Å amu$^{1/2}$. From Figure 2, one can see a strong sign dependence of the calculated absorption spectra. We should note here that compared with the $\varphi = 0$ case, in the negative sign case the calculated absorption spectra become broader toward the high-energy region but there is no significant change in the lower energy region. On the other hand, the positive sign case shows drastic broadening toward both lower and higher energy regions.

B. Real Molecular Systems. $\pi-\pi^*$ electronic transitions in small organic molecules represent an important example of the systems where the Duschinsky rotation between the ground and excited electronic states is extremely large. In this paper, we consider two molecules, ethylene (C_2H_4) and allene (C_3H_4), but a similar behavior can be also expected for their substituted analogues and for other linear unsaturated hydrocarbons with π bonds. Vibronic spectra of ethylene in the region of 6−8 eV have been a subject of numerous experimental[76−78] and theoretical[63,64,79−87] studies. The traditional assignment attributes the broad featureless underlying continuum in the spectra to the $\pi-\pi^*$ excitation to a $^1B_{1u}$ state. This continuum spreads from the energies below 50 000 cm^{-1} to at least 70 000 cm^{-1}. The absorption bands corresponding to the $\pi-\pi^*$ transition in allene have a similar weak, broad, and featureless character.[76,88−90] A weak absorption starts at ∼38 000 cm^{-1} and spreads to 52 000 cm^{-1} with eventual increase of intensity. For allene, two symmetry-forbidden $^1A_2 \leftarrow {}^1A_1$ and $^1B_1 \leftarrow {}^1A_1$ $\pi-\pi^*$ transitions can contribute through an intensity-borrowing mechanism from the allowed $^1E \leftarrow {}^1A_1$ ($\pi-3s$) and $^1B_2 \leftarrow {}^1A_1$ ($\pi-\pi^*$) transitions. Interestingly, recent [2 + 1] REMPI measurements of two-photon absorption spectra of allene[91] show the presence of the underlying continuum band at energies as high as 60000−75000 cm^{-1}. Let us consider now what can make the $\pi-\pi^*$ absorption spectra in ethylene and allene so broad and continuous and what the role of the Duschinsky effect is.

Theoretical $^1B_{1u} \leftarrow {}^1A_g$ ($\pi-\pi^*$) Absorption Spectra of Ethylene. It is well-known that the $^1B_{1u}$ ($\pi-\pi^*$) excited state of C_2H_4 is stabilized by D_2 torsion according to the Walsh rules.[92] As a result, geometry optimization of this state at the CIS/6-311(2+)G* and CASSCF/6-311(2+)G* levels with active spaces from (2,11) to (10,15)[63] gives a 90° twisted structure of D_{2d} symmetry (see Figure 3). This result is in agreement with previous findings by other authors.[79,83,84] Thus, the geometry change from the ground to excited state is very large. According to our calculations at the MRCI/ANO(2+) level,[64] the difference between the adiabatic (5.45 eV) and vertical (8.13 eV) excitation energies reaches ∼2.7 eV. Vibrational frequencies calculated at the CASSCF and CIS levels[63,64] for the ground and excited states, respectively, are shown in Table 1. Within the D_2 symmetry group common for all the states, the normal modes include four modes of "a" symmetry ($\nu_1 - \nu_4$), two modes of b_3 symmetry (ν_5, ν_6), three modes of b_1 symmetry ($\nu_7 - \nu_9$), and three modes of b_2 symmetry ($\nu_{10} - \nu_{12}$). Table 2 shows

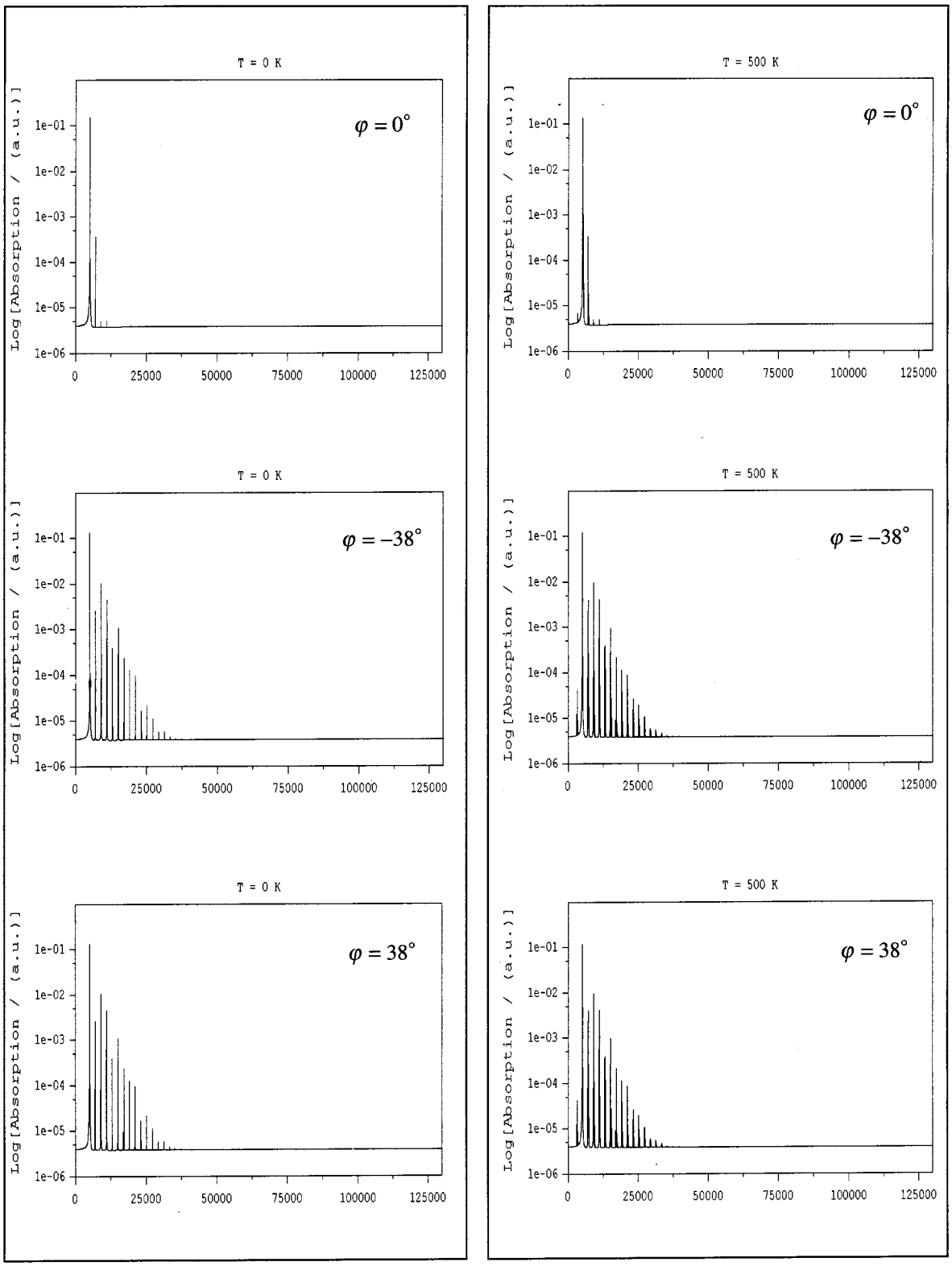

Figure 1. Effect of mode mixing on the absorption spectra of a distorted and rotated system. The right and left panels show the calculated absorption spectra at 0 and 500 K, respectively. In each panel, the top, middle, and bottom panels demonstrate the absorption spectra as a function of φ.

mass-weighted normal coordinates $|L|$ for the ground state. Graphical presentation of all normal modes was given earlier.[63] In the $\pi-\pi^*$ state, several modes change frequencies significantly compared to the ground state, for instance, C−C stretching coupled with HCH scissoring (ν_2, 1580 → 1398 cm^{-1}), CH_2 twisting (ν_4, 977 → 855 cm^{-1}), CCH bending (ν_8, 1205 → 912 cm^{-1}), CH_2 wagging (ν_9, 860 → 661 cm^{-1}), asymmetric CH stretching (ν_{10}, 3059 → 2841 cm^{-1}), and CCH bending (ν_{12}, 795 → 661 cm^{-1}). Only symmetric "a" modes are displaced; ΔQ values are large and the largest of them, 1.27 Å $amu^{1/2}$, is calculated for CH_2 twisting, ν_4, because in the $\pi-\pi^*$ state the molecule is twisted by 90°. The calculation of the Huang−Rhys factors S, $S = (^1/_2)(^\omega/_\hbar)(\Delta Q)^2$, for the $\nu_1 - \nu_4$ modes gives values of 7.45, 4.94, 1.55, and 22.49, respectively. Additionally, the normal coordinates are mixed, as seen from the rotational Duschinsky matrix $|\mathbf{C}|$ (Table 3). The rotated

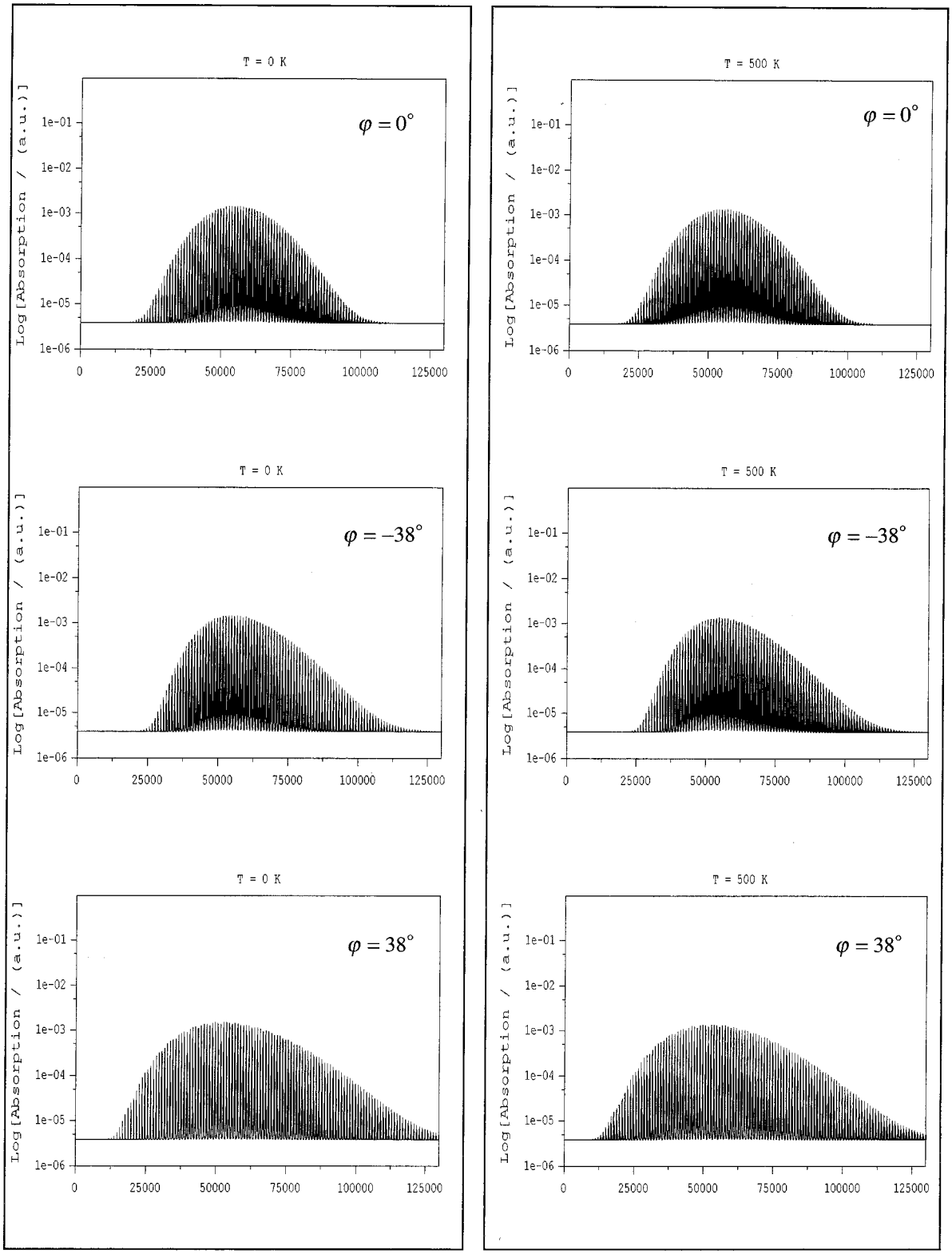

Figure 2. Calculated absorption spectra for a model system consisting of two displaced−distorted−rotated harmonic potentials.

normal modes of "a" symmetry (in D_2) for the ground and excited states are illustrated in Figure 4.

Now we use these data to compute the temperature dependence of the absorption spectrum for $^1B_{1u} \leftarrow {}^1A_g$ ($\pi-\pi^*$) of ethylene using our newly developed formalism. For this purpose, we develop an analytic expression for the computation of eq 9 for a two-mode mixing case (see Appendixes A and B). From Table 3, one can see that the Q_1 and Q_4 modes are strongly mixed with the Q_1' and Q_4' modes. For simplicity, we assume that only these two modes are mixed and that the rest are not mixed. In this case, the rotational Duschinsky matrix $|\mathbf{C}|$ can be approximated by a 2×2 matrix

$$\begin{pmatrix} 0.7937 & 0.6083 \\ -0.6083 & 0.7937 \end{pmatrix}$$

For computation, we use the fast Fourier transform algorithm with 262 144 points to generate the correlation function eq 4.

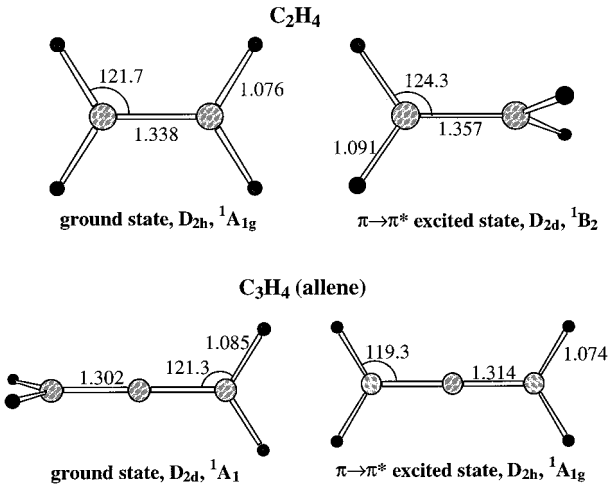

Figure 3. Optimized geometries of ethylene (ref 63) and allene (ref 68) in the ground and $\pi-\pi^*$ excited electronic states.

TABLE 1: Vibrational Frequencies (cm^{-1}) of C_2H_4 in the Ground and Excited States[a]

assignment	^1A_g (D_{2h})		$^1B_2$ (D_{2h})		symmetry in D_2
ν_1 CH stretch	a_g	2979	a_1	2828	a
ν_2 CC stretch	a_g	1580	a_1	1398	a
ν_3 CH_2 scissors	a_g	1286	a_1	1227	a
ν_4 CH_2 twisting	a_u	977	b_1	855	a
ν_5 CH stretch	b_{1u}	2960	b_2	2798	b_1
ν_6 CH_2 scissors	b_{1u}	1435	b_2	1274	b_1
ν_7 CH stretch	b_{3g}	3032	e	2841	b_3
ν_8 CCH bend	b_{3g}	1205	e	912	b_3
ν_9 CH_2 wagging	b_{3u}	860	e	661	b_3
ν_{10} CH stretch	b_{2u}	3059	e	2841	b_2
ν_{11} CH_2 wagging	b_{2g}	813	e	912	b_2
ν_{12} CCH bend	b_{2u}	795	e	661	b_2

[a] Calculated at the RHF/6-311(2+)G* and CIS/6-311(2+)G* levels, respectively, and scaled by 0.9 (from ref 63).

The frequency resolution is set to be 1 cm^{-1}, and we employ 1 cm^{-1} as a convergence factor. This factor does not influence the results, since its value is only 0.15% of the lowest vibrational frequency of this system.

The upper and lower panels in Figure 5 show an overview of the absorption spectra of ethylene at 0 and 500 K calculated using eqs B3 and C1. The upper and lower panels on the left side of Figure 6 show the calculated absorption spectra of ethylene at 0 and 500 K in the spectral region of 46000−57000 cm^{-1}. In the upper panel, one can see obvious vibronic structure with energy spacing of 855 cm^{-1}. This structure arises from the CH_2 twisting mode. One can also see that the vibronic structure starts from about 47 300 cm^{-1} . New peaks appear at energy lower than 47 300 cm^{-1} in the case of 500 K. These peaks are due to the thermal populations of the vibrational levels of the ground electronic state.

For comparison, we also demonstrate absorption spectra without the Duschinsky effect and they are shown in the upper and lower panels on the right side of Figure 6. From Figure 6, one can see that the vibronic structure and the temperature effect are very different from transitions with the Duschinsky effect.

Figure 7 shows a comparison of the calculated spectrum with the observed spectrum of $^1B_{1u} \leftarrow {}^1A_g$ ($\pi-\pi^*$) absorption spectra of ethylene.[77] One can see a good agreement in the vibronic structures between the calculated and observed spectra. Thus, our study supports the assignment of the underlying continuum in the ethylene absorption spectra to the $^1B_{1u} \leftarrow {}^1A_g$ ($\pi-\pi^*$) electronic transition and does not confirm the suggestion by Ryu and Hudson[87] that the continuum band also involves the $^1B_{1g} \leftarrow {}^1A_g$ ($\pi-3p_y$) transition. Also, the band is assigned in terms of four normal modes $Q_1 - Q_4$ of "a" symmetry (in the D_2 group), which is against the hypothesis of Siebrand et al.[82] who additionally invoked for the assignment a nonsymmetric b_{2g} normal mode (CH_2 wagging) active in intensity borrowing from the $^1B_{3u}$ ($\pi-3s$) state. Our calculations demonstrate that only a small fraction (~9.1%) of the total intensity for the $\pi-\pi^*$ transition corresponds to the 6−8 eV energy region. This explains an apparent contradiction between the calculated oscillator strengths for $\pi-\pi^*$ (0.36 at the EOM-CCSD level)[64] and $\pi-3s$ (0.08) and experimental absorption spectra where the distinct peaks due to $\pi-3s$ are more intense than the underlying continuum.

Theoretical $^1B_{1u} \rightarrow {}^1A_{1g}$ Internal Conversion Rate Constant of Ethylene. Now we calculate the internal conversion (IC) rate constant of the nonradiative transition $^1B_{1u} \rightarrow {}^1A_g$ of ethylene. In this case, there exist two promoting modes, Q_5 and Q_6, and the electronic coupling constants associated with these modes are given by 0.0038 $Å^{-1}$ $amu^{-1/2}$ and 0.072 $Å^{-1}$ $amu^{-1/2}$, respectively.[30] To calculate the internal conversion rate, we use eqs 19, B3, C1, and D1 with the 2 × 2 rotational Duschinsky matrix

$$\begin{pmatrix} 0.7937 & -0.6083 \\ 0.6083 & 0.7937 \end{pmatrix}$$

Figure 8 shows the calculated temperature dependence of the internal conversion rate constants of the nonradiative transition $^1B_{1u} \rightarrow {}^1A_g$ of ethylene. One can see in Figure 8 that the IC rate constants show a moderate temperature dependence in the temperature range 0−1500 K.

In a previous study, we reported the IC rate constants for these two modes at 0 K using only displaced potential surfaces for the promoting modes, and they were 7.39 × 10^6 s^{-1}(Q_5) and 1.26 × 10^9 s^{-1} (Q_6).[30] In this present work, displaced−distorted potential surfaces for the promoting modes have been used.

Theoretical $^1B_1 \leftarrow {}^1A_1$ ($\pi-\pi^*$) Absorption Spectra of Allene. Earlier,[68] we carried out ab initio calculations of the ground and excited states of allene, where the geometries were optimized at the CASSCF/6-311+G** and density functional[93,94] B3LYP/6-311G** levels and the energies were refined using the MRCI/ANO(2+) approach. In allene, the ground electronic state has D_{2d} symmetry (see Figure 3); so two CH_2 groups are twisted with respect to each other by 90°. The excited $\pi-\pi^*$ $^1B_1$ (D_{2d}) state is stabilized by D_2 torsion according to the Walsh rules.[92,95,96] The doubly occupied 2e and virtual 3e* MOs in D_{2d} symmetry split into in-plane σ and out-of-plane π components, with the energies and symmetries such that $b_{3u}(\pi) < b_{2g}(\pi) < b_{2u}(\sigma^*) < b_{3u}(\pi^*)$ for the $D_{2d} \rightarrow D_2 \rightarrow D_{2h}$ transformation. On the basis of Walsh's rules, the σ^* A_u state ($b_{2g}(\pi)b_{2u}(\sigma^*)$) is the stabilized form of the B_1 Franck−Condon state. However, as shown by MRCI calculations,[68] because B_1 collapses to the totally symmetric representation (A) at intermediate D_2 geometries, the ground state (1^1A_1) ultimately correlates with the open-shell ^1A_u state and the excited $^1B_1$ state with the closed-shell excited state $(1b_{3u})^2(1b_{2g})^2$ ^1A_g. Thus, ^1A_g is the first excited state at the D_{2h} geometry[68,97] (Figure 3). Except for the CH_2 twisting, the other geometric changes from $^1A_1$ (D_{2d}) to ^1A_g (D_{2h}) are minor. According to MRCI calculations, the adiabatic excitation energy for S_1 is only 3.02 eV (24 342 cm^{-1}), about 3 eV lower than the vertical excitation energies for $^1A_2$ (6.10 eV) and $^1B_1$ (6.55 eV) at D_{2d} symmetry.[68] Scaled[98] vibrational frequencies for the ground $^1A_1$ (D_{2d}) and excited ^1A_g (D_{2h}) electronic states calculated at the B3LYP/6-

TABLE 2: Normal Modes of C_2H_4 in the Ground State[a]

mode sym		Q_{12} b_{2u}	Q_9 b_{3u}	Q_{11} b_{2g}	Q_4 a_u	Q_8 b_{3g}	Q_3 a_g	Q_6 b_{1u}	Q_2 a_g	Q_5 b_{1u}	Q_1 a_g	Q_7 b_{3g}	Q_{10} b_{2u}
C^1,	x	0.00	0.27	0.43	0.00	0.00	0.00	0.00	0.00	0.00	0.00	0.00	0.00
	y	−0.13	0.00	0.00	0.00	0.43	0.00	0.00	0.00	0.00	0.00	−0.23	0.23
	z	0.00	0.00	0.00	0.00	0.00	0.33	0.23	0.59	0.14	−0.19	0.00	0.00
C^2,	x	0.00	0.27	−0.43	0.00	0.00	0.00	0.00	0.00	0.00	0.00	0.00	0.00
	y	−0.13	0.00	0.00	0.00	−0.43	0.00	0.00	0.00	0.00	0.00	0.23	0.23
	z	0.00	0.00	0.00	0.00	0.00	−0.33	0.23	−0.59	0.14	0.19	0.00	0.00
H^1,	x	0.00	−0.46	−0.40	0.50	0.00	0.00	0.00	0.00	0.00	0.00	0.00	0.00
	y	0.23	0.00	0.00	0.00	−0.11	−0.17	0.27	0.23	−0.42	0.41	0.40	−0.40
	z	−0.43	0.00	0.00	0.00	0.38	0.41	−0.39	−0.15	−0.25	0.25	0.25	−0.25
H^2,	x	0.00	−0.46	−0.40	−0.50	0.00	0.00	0.00	0.00	0.00	0.00	0.00	0.00
	y	0.23	0.00	0.00	0.00	−0.11	0.17	−0.27	−0.23	0.42	−0.41	0.40	−0.40
	z	0.43	0.00	0.00	0.00	−0.38	0.41	−0.39	−0.15	−0.25	0.25	−0.25	0.25
H^3,	x	0.00	−0.46	0.40	−0.50	0.00	0.00	0.00	0.00	0.00	0.00	0.00	0.00
	y	0.23	0.00	0.00	0.00	0.11	−0.17	−0.27	0.23	0.42	0.41	−0.40	−0.40
	z	0.43	0.00	0.00	0.00	0.38	−0.41	−0.39	0.15	−0.25	−0.25	0.25	0.25
H^4,	x	0.00	−0.46	0.40	0.50	0.00	0.00	0.00	0.00	0.00	0.00	0.00	0.00
	y	0.23	0.00	0.00	0.00	0.11	0.17	0.27	−0.23	−0.42	−0.41	−0.40	−0.40
	z	−0.43	0.00	0.00	0.00	−0.38	−0.41	−0.39	0.15	−0.25	−0.25	−0.25	−0.25

[a] From ref 63.

TABLE 3: Duschinsky Matrix and Normal Mode Displacements ΔQ (in Å amu$^{1/2}$) for the $^1B_2-{}^1A_g$ Transition in C_2H_4

	Q_1	Q_2	Q_3	Q_4
Q_1'	0.7977	−0.1467	−0.0027	0.5780
Q_2'	0.0887	−0.8622	−0.3802	−0.3153
Q_3'	−0.1024	0.2951	−0.9156	0.2364
Q_4'	−0.5850	−0.3823	0.1259	0.7195
ΔQ	0.416	0.469	0.286	1.273

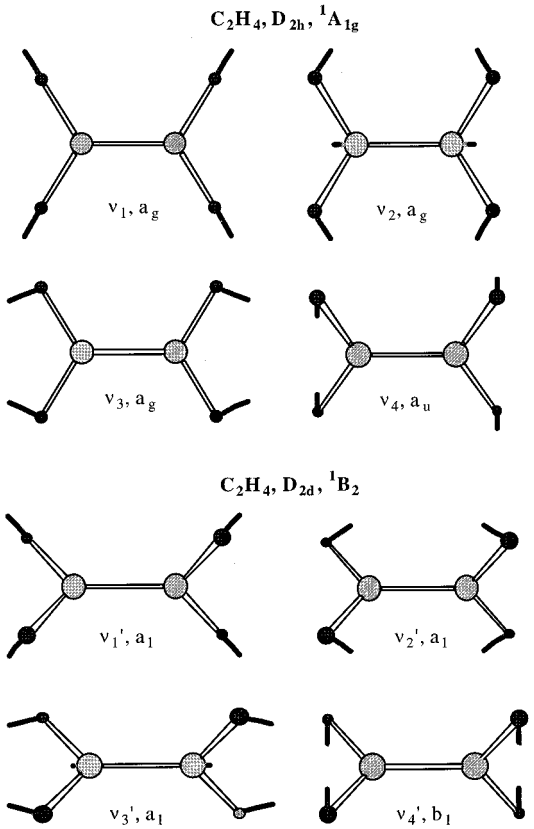

Figure 4. Normal modes of ethylene in the ground (D_{2h},^1A_g) and excited (D_{2d},$^1B_2$) electronic states participating in the Duschinsky rotation.

311G** level are presented in Table 4, and a numerical presentation of the normal modes in terms of displacements of Cartesian coordinates is given in Table 5. All normal modes for the ground electronic state are shown in Figure 9a and the rotated normal modes of "a" symmetry (within the D_2 group) for the excited state are illustrated in Figure 9b.

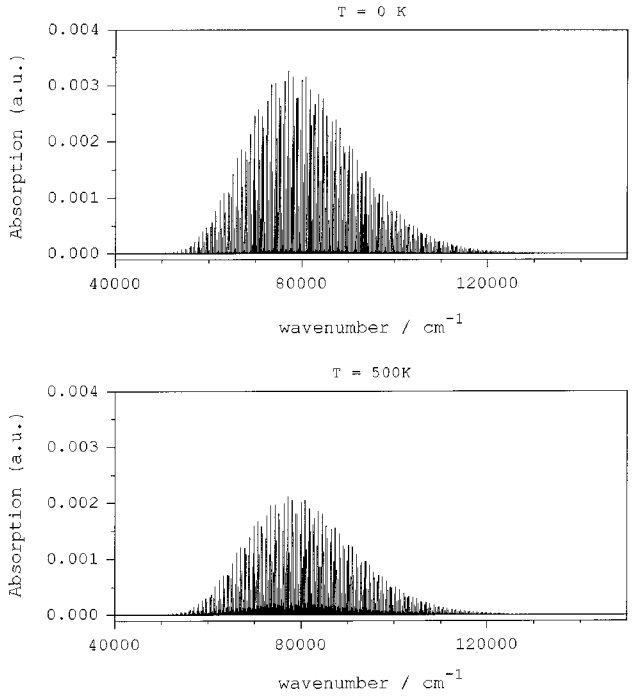

Figure 5. Overview of the absorption spectra calculated for $^1B_{1u} \leftarrow {}^1A_g$ ($\pi-\pi^*$). The upper and lower panels show the calculated absorption spectra at 0 and 500 K, respectively.

Our density functional calculation shows a significant distortion of normal modes (frequency change) from the ground to the excited state. The frequencies ν_{12} and ν_{13} corresponding to out-of-plane CH_2 wagging decrease in ^1A_g from 833 to 148 and 102 cm^{-1}. While the b_2 component of the CH_2 in-plane wagging frequency ν_{10-11} remains almost unchanged, the corresponding b_3 frequency decreases from 978 to 490 cm^{-1} in the excited state. For the CCH bending frequency ν_{14-15}, the b_3 component increases from 357 to 502 cm^{-1} and the b_2 component decreases by about 60 cm^{-1}. The CH_2 symmetric scissoring ν_2, CC asymmetric stretch ν_6, and CH_2 asymmetric scissoring ν_7 decrease their frequencies in ^1A_g by ∼150 cm^{-1}. The normal mode displacement occurs only for the modes Q_1-Q_4, which belong to the totally symmetric irreducible representation "a" of the symmetry group D_2, common for the ground and excited-state geometries. In general, the displacements are similar to those found in ethylene (see Table 3 for comparison). The mode Q_4 corresponding to CH_2 is displaced to the greatest extent ($\Delta Q_4 = 1.321$ Å amu$^{1/2}$). It is followed by symmetric CH stretching

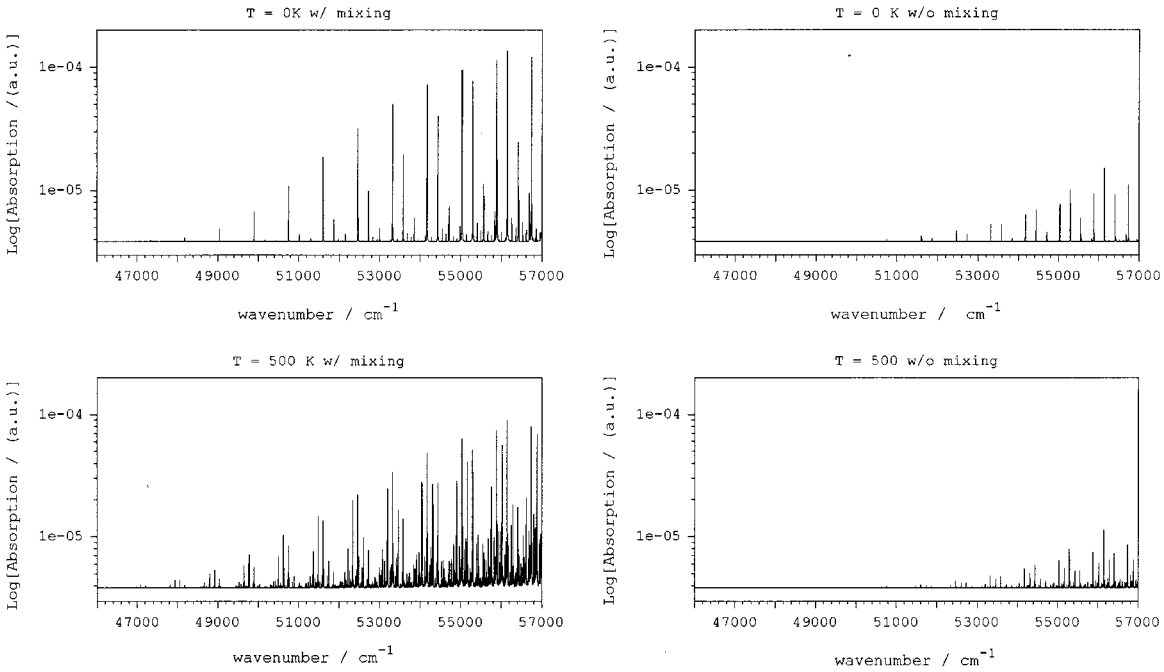

Figure 6. Comparison between mixing and no-mixing cases. The upper and lower panels of the left side show the calculated absorption spectra of ethylene at 0 and 500 K in the spectral region of 46000−57000 cm^{-1}, respectively. The two panels on the right side show the corresponding spectra without mixing.

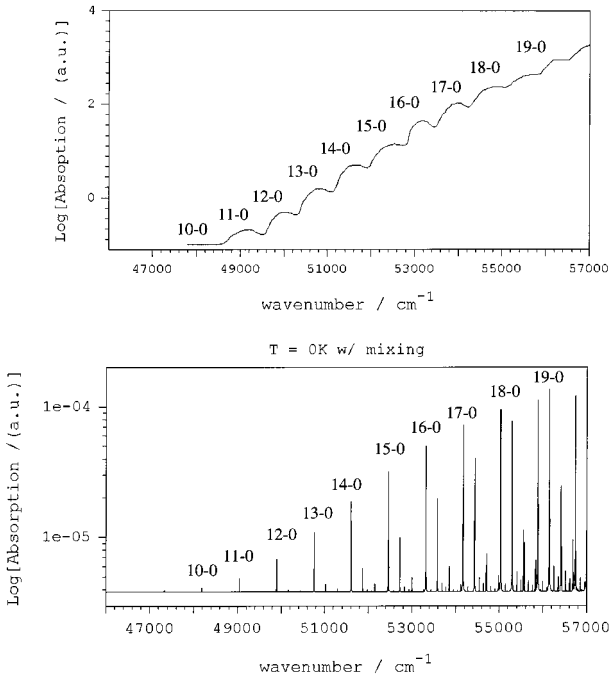

Figure 7. Comparison of the calculated spectrum with the observed $^1B_{1u} \leftarrow {}^1A_g$ ($\pi-\pi^*$) absorption spectrum of ethylene. The calculated and the observed spectra are shown in the lower and upper panels, respectively. The observed spectrum is taken from ref 77.

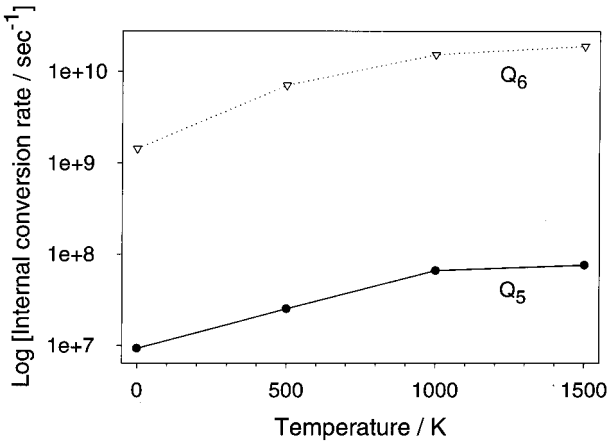

Figure 8. Temperature dependence of internal conversion rate constants of the nonradiative transition $^1B_{1u} \rightarrow {}^1A_g$ of ethylene. The dotted and the solid lines depict the IC rate constants for the promoting modes Q_6 and Q_5, respectively.

Q_1 ($\Delta Q_1 = 0.449$ Å amu$^{1/2}$) and symmetric CH_2 scissoring Q_2 ($\Delta Q_2 = 0.267$ Å amu$^{1/2}$).

Significant mode mixing is also found (Table 6). The Duschinsky matrix for the Q_1-Q_4 normal modes is similar to that for ethylene, except the mixing of Q_2 and especially Q_3 with the other normal coordinates is less pronounced. Only modes Q_1 (CH stretch) and Q_4 (CH_2 twisting) are heavily mixed with each other. In symmetry b_1 there is some rotation of Q_5 (CH stretch) and Q_7 (CH_2 asymmetric scissoring), while Q_6 (CC asymmetric stretch) is not mixed with other modes. In symmetries b_2 and b_3, the CH asymmetric stretch Q_{8-9} mixes with CH_2 out-of-plane wagging Q_{12-13} and, to a lesser extent, with CH_2 in-plane wagging Q_{10-11}. The CCH bending modes Q_{14-15} remain essentially unmixed with other normal coordinates. The Duschinsky matrices for symmetries a, b_2, and b_3 (parts a, c, and d of Table 6, respectively) as well as that for ethylene (Table 3) are unitary; the sum of squares for each row and column is equal to unity. On the other hand, the Duschinsky matrix for b_1 is not unitary; the sum of squares for the first row and the first column is substantially less than 1. At this point, we do not completely understand this result. A reason for it can be a mixing of vibrational normal coordinates in the ground state with rotational normal coordinates of the excited state. For instance, the mode corresponding to rotation around the *Z* axis (CCC) has symmetry b_{1g} in the excited state (D_{2h}) and a_2 in the ground state (D_{2d}), which correspond to b_1 in the common D_2 point group. This rotational mode can mix with vibrational normal modes of b_1 symmetry in the other electronic state. To our-

TABLE 4: Vibrational Frequencies (cm^{-1}) of Allene in the Ground and Excited States Calculated at the B3LYP/6-311G Level[a]**

assignment	$^1A_1$ (D_{2d})[a]		^1A_g (D_{2h})		symmetry in D_2
ν_1 CH sym stretch	a_1	3001 (2993)	a_g	3027	a
ν_2 CH_2 sym sciss.	a_1	1423 (1432)	a_g	1270	a
ν_3 CC sym stretch	a_1	1066 (1071)	a_g	1009	a
ν_4 CH_2 twisting	b_1	850 (820)	a_u	879[b]	a
ν_5 CH stretch	b_2	2997 (2960)	b_{1u}	3024	b_1
ν_6 CC asym stretch	b_2	1974 (1980)	b_{1u}	1823	b_1
ν_7 CH_2 asym sciss	b_2	1368 (1389)	b_{1u}	1210	b_1
ν_{8-9} CH asym stretch	e	3069 (3061)	b_{2u}	3096	b_2
			b_{3g}	3094	b_3
ν_{10-11} CH_2 in-plane wagging	e	978 (1031)	b_{2u}	966	b_2
			b_{3g}	490	b_3
ν_{12-13} CH_2 out-of-plane wagging	e	833 (838)	b_{3u}	148	b_3
			b_{2g}	102	b_2
ν_{14-15} CCH bend	e	357 (353)	b_{3u}	502	b_3
			b_{2u}	291	b_2

[a] Scaled by 0.9614 (ref 98). In parentheses are the experimental frequencies from ref 89. [b] This value is calculated at the CASSCF/6-311+G** level.

knowledge, such an interesting vibrational−rotational Duschinsky effect was not reported before, although the rotational Duschinsky effect is known,[32] and requires further investigation.

At this stage we use the calculated normal mode displacements, distortions, and rotations to compute the absorption spectra for allene. Although at the B3LYP level we find a large distortion effect in the frequency ν_4, this distortion effect is not reasonable. This is due to the fact that the DFT method failed for this particular vibrational mode. Thus, we recalculated this vibrational frequency numerically at the ab initio CASSCF/6-311+G** level and obtained the value of 879 cm^{-1} used for the calculation of the absorption spectra of $^1B_1 \leftarrow {}^1A_1$ ($\pi-\pi^*$).

We are now in a position to compute the temperature dependence of the absorption spectrum for the $^1B_1 \leftarrow {}^1A_1$ ($\pi-\pi^*$) transition of allene. From Table 6, one can see that the $Q_1$and Q_4 modes are strongly mixed with the Q'_1 and Q'_4 modes in group a, the Q'_5 and Q'_7 modes are strongly mixed with the Q'_5 and Q'_7 modes in group b, the Q'_8 and Q'_{13} modes are strongly mixed with the Q'_8 and Q'_{13} modes in group c, and the Q'_9 and Q'_{12} modes are strongly mixed with the Q'_9 and Q'_{12} modes in group d. For simplicity, we assume that only these modes are mixed and that the rest are not mixed. In this case, the rotational Duschinsky matrix $|\mathbf{C}|$ can be approximated by 2×2 matrices

$$\begin{pmatrix} 0.75075 & -0.5924 \\ 0.5924 & 0.75075 \end{pmatrix}$$

and

$$\begin{pmatrix} 0.8582 & 0.1398 \\ -0.1398 & 0.8582 \end{pmatrix}$$

$$\begin{pmatrix} 0.7489 & -0.6011 \\ 0.6011 & 0.7489 \end{pmatrix}$$

$$\begin{pmatrix} 0.7407 & -0.5994 \\ 0.5994 & 0.7407 \end{pmatrix}$$

respectively.

Figure 10 compares the calculated absorption spectra with and without mode mixing of $^1B_1 \leftarrow {}^1A_1$ ($\pi-\pi^*$) of allene. For the allene case, we cannot see the drastic change in the lower energy region of the absorption spectra, as can be seen in the ethylene case, but the spectrum becomes broader toward the higher energy region because of the Duschinsky effect. This feature can be explained by referring to the model calculation mentioned in the previous section. Note that only the modes in group a have displacements and the rest do not and that the 2×2 matrix for group a has the opposite sign compared with the ethylene case. It should be noted that one must be careful in determining the sign of Duschinsky matrix elements.

Theoretical $^1B_1 \rightarrow {}^1A_1$ Internal Conversion Rate Constant of Allene. It is instructive to investigate the temperature dependence of the internal conversion rate of the nonradiative transition $^1B_1 \rightarrow {}^1A_1$ of allene. For this calculation, we shall adopt the CC asymmetric stretch mode Q_6 as a promoting mode. The rotational Duschinsky matrix $|\mathbf{C}|$ for this calculation can be given by a 2×2 matrices

$$\begin{pmatrix} 0.75075 & 0.5924 \\ -0.5924 & 0.75075 \end{pmatrix}$$

$$\begin{pmatrix} 0.8582 & 0.1398 \\ -0.1398 & 0.8582 \end{pmatrix}$$

$$\begin{pmatrix} 0.7489 & 0.6011 \\ -0.6011 & 0.7489 \end{pmatrix}$$

and

$$\begin{pmatrix} 0.7407 & 0.5994 \\ -0.5994 & 0.7407 \end{pmatrix}$$

for groups a, b, c, and d, respectively.

Figure 11 shows the calculated temperature dependence of the internal conversion rate constants for the nonradiative transition $^1B_1 \rightarrow {}^1A_1$ of allene. These rate constants are normalized to the IC rate constant for the no-mixing case at $T = 0$ K. Although our ab initio calculations show (see Table 4) that allene has large frequency changes in groups c and d, these modes are only distorted−rotated. As already seen in the model calculations, the distortion effect alone cannot broaden the Franck−Condon factor distribution.

III. Conclusion

In this paper, we have described the important role of the Duschinsky effect for absorption spectra and radiationless transitions in polyatomic molecules. We demonstrated that this role can be analyzed through ab initio calculations of potential energy surfaces for the ground and excited electronic states. We have presented analytical expressions for calculating absorption coefficients and radiationless transitions that involve the Duschinsky effect. This effect is expected to be important for $\pi-\pi^*$ transitions for small and intermediate size molecules. In this paper, to demonstrate the importance of this effect, we have chosen ethylene and allene as examples. We have shown that in absorption spectroscopy the Duschinsky effect will, under certain conditions, introduce a significant broadening of the electronic spectra. The Duschinsky effect will also increase the rate of radiationless transitions.

It should be noted that intramolecular vibrational redistribution (IVR) can also cause broadening of FC bright states. This broadening is usually involved in the transient absorption or spontaneous and stimulated emission spectra of isolated (i.e., collision-free) molecules. For example, IVR can be observed in an isolated molecule by optical excitation using a UV laser to a high vibronic state (or states); IVR will take place by anharmonic coupling (and/or Coriolis coupling) in the excited electronic state. In this case, if the transient absorption (or emission) experiment is performed, then one can observe the transient spectral broadening due to IVR. On the other hand, when the excited molecule goes through internal conversion to the ground electronic state, the molecule will be highly

TABLE 5: Normal Modes of Allene in the Ground State

mode	sym	Q_1 a_1	Q_2 a_1	Q_3 a_1	Q_4 b_1	Q_5 b_2	Q_6 b_2	Q_7 b_2	Q_8 e	Q_9 e	Q_{10} e	Q_{11} e	Q_{12} e	Q_{13} e	Q_{14} e	Q_{15} e
C^1,	*x*	0.00	0.00	0.00	0.00	0.00	0.00	0.00	0.16	0.16	−0.20	−0.26	−0.24	0.27	0.07	−0.24
	y	0.00	0.00	0.00	0.00	0.00	0.00	0.00	0.16	0.16	−0.26	−0.20	0.27	−0.24	−0.24	0.07
	z	−0.17	0.40	0.56	0.00	0.17	−0.39	0.17	0.00	0.00	0.00	0.00	0.00	0.00	0.00	0.00
C^2,	*x*	0.00	0.00	0.00	0.00	0.00	0.00	0.00	0.00	0.00	0.00	0.40	0.09	0.00	0.00	0.73
	y	0.00	0.00	0.00	0.00	0.00	0.00	0.00	0.00	0.00	0.40	0.00	0.00	0.09	0.73	0.00
	z	0.00	0.00	0.00	0.00	−0.03	0.82	0.17	0.00	0.00	0.00	0.00	0.00	0.00	0.00	0.00
C^3,	*x*	0.00	0.00	0.00	0.00	0.00	0.00	0.00	−0.16	0.16	0.20	−0.26	−0.24	−0.27	−0.07	−0.24
	y	0.00	0.00	0.00	0.00	0.00	0.00	0.00	0.16	−0.16	−0.26	0.20	−0.27	−0.24	−0.24	−0.07
	z	0.17	−0.40	−0.56	0.00	0.17	−0.39	0.17	0.00	0.00	0.00	0.00	0.00	0.00	0.00	0.00
H^1,	*x*	0.30	0.18	−0.05	0.35	−0.30	−0.05	0.18	−0.28	−0.28	0.11	0.09	0.30	−0.30	−0.02	−0.21
	y	0.30	0.18	−0.05	−0.35	−0.30	−0.05	0.18	−0.28	−0.28	0.09	0.11	−0.30	0.30	−0.21	−0.02
	z	0.25	−0.32	0.30	0.00	−0.25	−0.04	−0.40	−0.25	−0.25	−0.37	−0.37	0.01	0.01	0.20	0.20
H^2,	*x*	−0.30	−0.18	0.05	−0.35	0.30	0.05	−0.18	−0.28	−0.28	0.11	0.09	0.30	−0.30	−0.02	−0.21
	y	−0.30	−0.18	0.05	0.35	0.30	0.05	−0.18	−0.28	−0.28	0.09	0.11	−0.30	0.30	−0.21	−0.02
	z	0.25	−0.32	0.30	0.00	−0.25	−0.04	−0.40	0.25	0.25	0.37	0.37	−0.01	−0.01	−0.20	−0.20
H^3,	*x*	−0.30	−0.18	0.05	−0.35	−0.30	−0.05	0.18	0.28	−0.28	−0.11	0.09	0.30	0.30	0.02	−0.21
	y	0.30	0.18	−0.05	−0.35	0.30	0.05	−0.18	−0.28	0.28	0.09	−0.11	0.30	0.30	−0.21	0.02
	z	−0.25	0.32	−0.30	0.00	−0.25	−0.04	−0.40	0.25	−0.25	0.37	−0.37	0.01	−0.01	−0.20	0.20
H^4,	*x*	0.30	0.18	−0.05	0.35	0.30	0.05	−0.18	0.28	−0.28	−0.11	0.09	0.30	0.30	0.02	−0.21
	y	−0.30	−0.18	0.05	0.35	−0.30	−0.05	0.18	−0.28	0.28	0.09	−0.11	0.30	0.30	−0.21	0.02
	z	−0.25	0.32	−0.30	0.00	−0.25	−0.04	−0.40	−0.25	0.25	−0.37	0.37	−0.01	0.01	0.20	−0.20

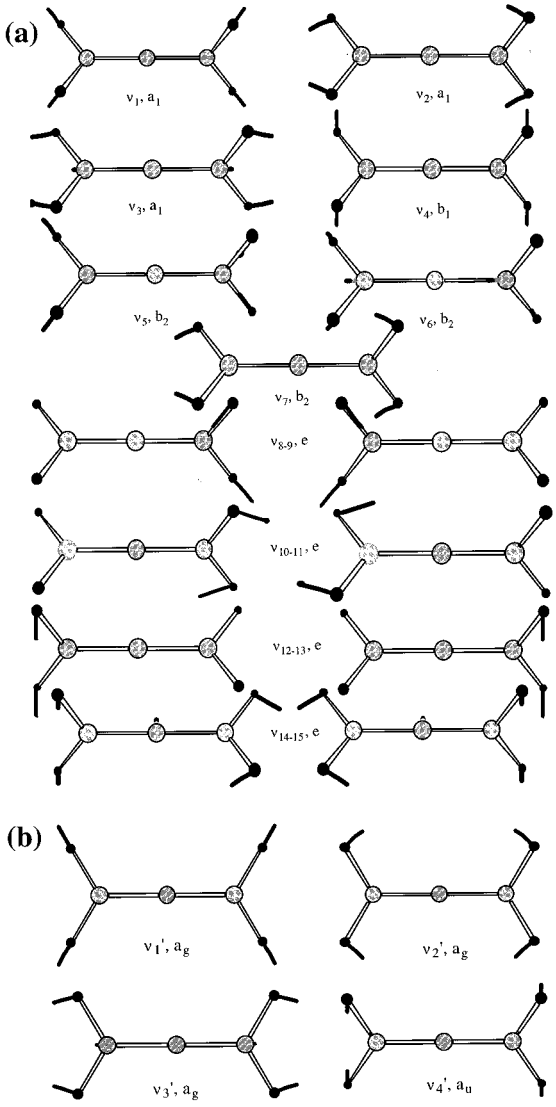

Figure 9. (a) Normal modes of allene in the ground electronic state (D_{2d},$^1A_1$). (b) Normal modes of a_g and a_u symmetries in the excited electronic state of allene (D_{2h},$^1A_{1g}$) mixing with the a_1 and b_1 normal modes in the ground state.

vibrationally excited; IVR can also take place in the ground electronic state, and again, the transient spectral broadening can be observed. In this paper, we are concerned with the absorption

TABLE 6: Duschinsky Matrices and Normal Mode Displacements ΔQ (in Å amu$^{1/2}$) for the $^1A_g-^1A_1$ Transition in Allene

(a) Normal Modes of Symmetry "a" (D_2)

	Q_1	Q_2	Q_3	Q_4
Q_1'	0.7944	−0.1382	0.0250	−0.5936
Q_2'	−0.1333	0.9184	0.1084	−0.3644
Q_3'	0.0365	−0.0642	0.9878	0.1309
Q_4'	0.5912	0.3673	0.0906	0.7071
ΔQ	0.449	0.267	0.085	1.321

(b) Normal Modes of Symmetry b_1 (D_2)

	Q_5	Q_6	Q_7
Q_5'	0.7947	−0.0440	0.1379
Q_6'	−0.0397	0.9944	0.0225
Q_7'	0.1417	0.0127	0.9217

(c) Normal Modes of Symmetry b_2 (D_2)

	Q_8	Q_{10}	Q_{13}	Q_{15}
Q_8'	0.7831	0.1166	−0.6001	0.0145
Q_{10}'	−0.0711	−0.8623	−0.3068	−0.3913
Q_{13}'	0.6021	−0.3419	0.7147	0.0809
Q_{15}'	−0.1063	−0.3346	−0.1866	0.9130

(d) Normal Modes of Symmetry b_3 (D_2)

	Q_9	Q_{11}	Q_{12}	Q_{14}
Q_9'	−0.7831	−0.1036	−0.5961	0.1476
Q_{11}'	−0.1077	−0.8134	0.4038	0.3889
Q_{12}'	0.6027	−0.3708	−0.6983	0.1294
Q_{14}'	0.0815	0.4343	0.0287	0.8966

spectra originating from the ground electronic state. Since the Boltzmann average is included in the absorption coefficient [see eq 11], it means that collisions do exist to maintain vibrational equilibrium, and the spectral broadening due to IVR does not have any contribution in this case.

A main purpose of this paper is to show how the experimental results of spectroscopy and dynamics of molecules can be analyzed by ab initio calculations. It should be emphasized that the performance of ab initio methods in producing detailed features of potential energy surfaces can be checked from the measurements of high-resolution spectroscopy and single-vibronic-level lifetimes. In other words, rapid progress in the understanding of photophysical properties and photophysical processes can be made when ab initio calculations of photophysical properties and processes are carried out in the analysis of the experimental results. In particular, one of the most important physical properties of the molecule is its degrees of freedom of nuclear motion. Because of this property, the absorption spectra of molecules exhibit structures. Radiationless

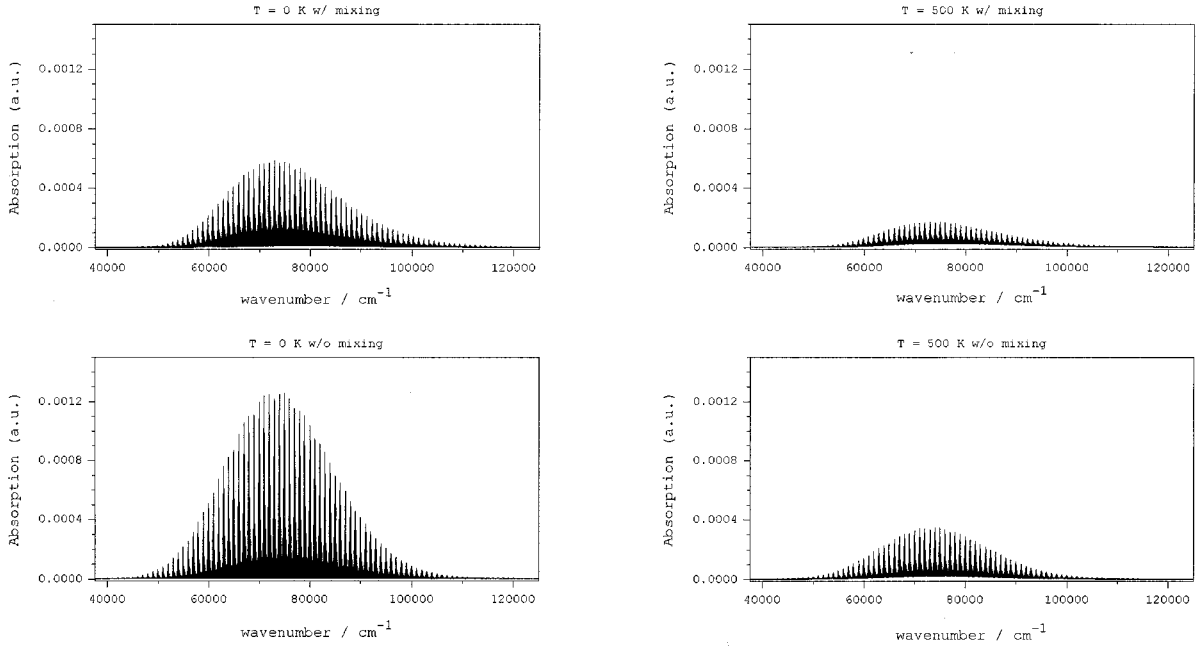

Figure 10. Calculated absorption spectra with and without mode mixing of $^1B_1 \leftarrow {}^1A_1$ ($\pi-\pi^*$) of allene. The upper and lower panels show the calculated spectra with and without mode mixing. The spectra shown in the left and right panels are calculated for $T = 0$ and $T = 500$ K, respectively.

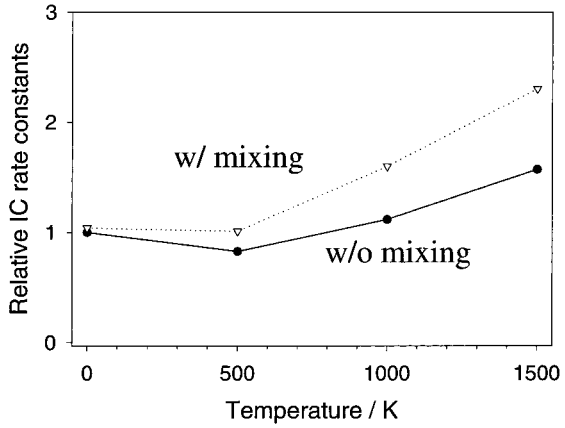

Figure 11. Temperature dependence of internal conversion rate constants of the nonradiative transition $^1B_1 \rightarrow {}^1A_1$ of allene. The dashed and solid lines denote the calculated IC rate constants for mixing and no-mixing cases, respectively. The IC rate constants are normalized with the IC rate constant for the no-mixing case at $T = 0$ K.

transitions can take place also because of the coupling between electronic and nuclear motions. We emphasize here that the vibrational information provided by ab initio calculations is as important as electronic information. For example, as already seen in this work, a few large displacements and rotations of the relevant potential surfaces become extremely important for the absorption spectra and the rate constants of radiationless transitions. With vibrational information, to analyze the observed results, one can theoretically construct the structure of absorption spectra and/or calculate the rate constants of radiationless transitions as a function of energy. This, in turn, encourages theoreticians to fine-tune ab initio calculation methods for the potential energy surfaces and thus for the molecular structures of electronically excited states or even cations and anions. Furthermore, ab initio calculations can also help us understand the photodissociation of molecules, especially for the case in which the electronically excited molecule (due to, say, optical absorption) goes through radiationless transitions to the ground electronic state where the hot molecule decomposes.

Acknowledgment. This work was supported by the National Science Council of R.O.C. (in part under Grant NSC 8902113-M-001-034) and Academia Sinica. A partial support from the Petroleum Research Fund of the Republic of China is also appreciated. The authors thank the referees for their helpful suggestions and corrections.

Appendix A

In this appendix, we shall derive expressions for the correlation function $G(t)$ for several cases. First, let us consider a two-mixing-mode case in which only modes 1 and 2 exhibit the Duschinsky effect. In this case,

$$G(t) = G_{12}(t)\prod_{l=1}^{l\neq 1,2} G_l(t) \tag{A1}$$

where

$$G_l(t) = \sum_{\nu_l}\sum_{\nu_l'} P_{a\nu_l}|\langle\chi_{b\nu_l'}(Q_l')|\chi_{a\nu_l}(Q_l)\rangle|^2 \exp\left[it\left\{\left(\nu_l' + \frac{1}{2}\right)\omega_l' - \left(\nu_l + \frac{1}{2}\right)\omega_l\right\}\right] \tag{A2}$$

and

$$G_{12}(t) = \sum_{\nu_1}\sum_{\nu_2}\sum_{\nu_{\alpha_1}'}\sum_{\nu_{\alpha_2}'} P_{a\nu_1\nu_2}|\langle\chi_{b\nu_{\alpha_1}'}(Q_{\alpha_1}')\chi_{b\nu_{\alpha_2}'}(Q'_{\alpha_2})|\chi_{a\nu_1}(Q_1) \times \chi_{a\nu_2}(Q_2)\rangle|^2 \exp\left[it\left\{\left(\nu_{\alpha_1}' + \frac{1}{2}\right)\omega_{\alpha_1}' + \left(\nu_{\alpha_2}' + \frac{1}{2}\right)\omega_{\alpha_2}' - \left(\nu_1 + \frac{1}{2}\right)\omega_1 - \left(\nu_2 + \frac{1}{2}\right)\omega_2\right\}\right] \tag{A3}$$

Applying the Slater sum to eq A3 leads to

$$G_{12}(t) = \frac{2\sinh\frac{\hbar\omega_1}{2kT}\,2\sinh\frac{\hbar\omega_2}{2kT}\sqrt{\beta_1\beta_2\beta_{\alpha 1}\beta'_{\alpha 2}}}{\sqrt{2^4\pi^4\sinh\lambda_1\sinh\lambda_2\sinh\mu'_{\alpha 1}\sinh\mu'_{\alpha 2}}} \times \int_{-\infty}^{\infty} dQ_1 \int_{-\infty}^{\infty} d\bar{Q}_1 \int_{-\infty}^{\infty} dQ_2 \int_{-\infty}^{\infty} d\bar{Q}_2 \times$$

$$\exp\left[-\frac{\beta_1}{4}\left\{(Q_1+\bar{Q}_1)^2\tanh\frac{\lambda_1}{2}+(Q_1-\bar{Q}_1)^2\coth\frac{\lambda_1}{2}\right\}\right]\times$$

$$\exp\left[-\frac{\beta_2}{4}\left\{(Q_2+\bar{Q}_2)^2\tanh\frac{\lambda_2}{2}+(Q_2-\bar{Q}_2)^2\coth\frac{\lambda_2}{2}\right\}\right]\times$$

$$\exp\left[-\frac{\beta'_{\alpha 1}}{4}\left\{(Q'_{\alpha 1}+\bar{Q}'_1)^2\tanh\frac{\mu'_{\alpha 1}}{2}+(Q'_{\alpha 1}-\bar{Q}'_{\alpha 1})^2\coth\frac{\mu'_{\alpha 1}}{2}\right\}\right]\times$$

$$\exp\left[-\frac{\beta'_{\alpha 2}}{4}\left\{(Q'_{\alpha 2}+\bar{Q}'_{\alpha 2})^2\tanh\frac{\mu'_{\alpha 2}}{2}+(Q'_{\alpha 2}-\bar{Q}'_{\alpha 2})^2\coth\frac{\mu'_{\alpha 2}}{2}\right\}\right] \quad \text{(A4)}$$

where $\lambda_1 = i\omega_1 + \hbar\omega_1/(kT)$, $\lambda_2 = i\omega_2 + \hbar\omega_2/(kT)$, $\mu'_{\alpha_1} = -i\omega'_{\alpha_1}$, $\mu'_{\alpha_2} = -i\omega'_{\alpha_2}$, and

$$Q'_{\alpha_1} = C_{\alpha_1 1}(Q_1+\Delta Q_1) + C_{\alpha_1 2}(Q_2+\Delta Q_2) \quad \text{(5a)}$$

and

$$Q'_{\alpha_2} = C_{\alpha_2 1}(Q_1+\Delta Q_1) + C_{\alpha_2 2}(Q_2+\Delta Q_2) \quad \text{(A5b)}$$

We rewrite eq A4 as

$$G_{12}(t) = 4K_{12}\int_{-\infty}^{\infty}dQ_1\int_{-\infty}^{\infty}d\bar{Q}_1\int_{-\infty}^{\infty}dQ_2\int_{-\infty}^{\infty}d\bar{Q}_2\exp[-A_{11}(Q_1+\bar{Q}_1)^2 - A_{22}(Q_2+\bar{Q}_2)^2 - A_{12}(Q_1+\bar{Q}_1)(Q_2+\bar{Q}_2)]\exp[-A_1(Q_1+\bar{Q}_1) - A_2(Q_2+\bar{Q}_2)]\exp[-B_{11}(Q_1-\bar{Q}_1)^2 - B_{22}(Q_2-\bar{Q}_2)^2 - B_{12}(Q_1-\bar{Q}_1)(Q_2-\bar{Q}_2)]\exp[-D] \quad \text{(A6)}$$

where

$$A_{ii} = \frac{\beta_i}{4}\tanh\frac{\lambda_i}{2} + \frac{\beta'_{\alpha_1}}{4}(C_{\alpha_1 i})^2\tanh\frac{\mu'_{\alpha_1}}{2} + \frac{\beta'_{\alpha_2}}{4}(C_{\alpha_2 i})^2\tanh\frac{\mu'_{\alpha_2}}{2}, \quad \text{for } i = 1, 2 \quad \text{(A7a)}$$

$$A_{12} = \frac{\beta'_{\alpha_1}}{2}C_{\alpha_1 1}C_{\alpha_1 2}\tanh\frac{\mu'_{\alpha_1}}{2} + \frac{\beta'_{\alpha_2}}{2}C_{\alpha_2 1}C_{\alpha_2 2}\tanh\frac{\mu'_{\alpha_2}}{2} \quad \text{(A7b)}$$

$$B_{ii} = \frac{\beta_i}{4}\coth\frac{\lambda_i}{2} + \frac{\beta'_{\alpha_1}}{4}(C_{\alpha_1 i})^2\coth\frac{\mu'_{\alpha_1}}{2} + \frac{\beta'_{\alpha_2}}{4}(C_{\alpha_2 i})^2\coth\frac{\mu'_{\alpha_2}}{2}, \quad \text{for } i = 1, 2 \quad \text{(A8a)}$$

$$B_{12} = \frac{\beta'_{\alpha_1}}{2}C_{\alpha_1 1}C_{\alpha_1 2}\coth\frac{\mu'_{\alpha_1}}{2} + \frac{\beta'_{\alpha_2}}{2}C_{\alpha_2 1}C_{\alpha_2 2}\coth\frac{\mu'_{\alpha_2}}{2} \quad \text{(A8b)}$$

$$K_{12} = \frac{\sqrt{\beta_1\beta_2\beta'_{\alpha_1}\beta'_{\alpha_2}}\sinh\frac{\hbar\omega_1}{2kT}\sinh\frac{\hbar\omega_2}{2kT}}{\sqrt{2^4\pi^4\sinh\lambda_1\sinh\lambda_2\sinh\mu'_{\alpha_1}\sinh\mu'_{\alpha_2}}} \quad \text{(A9)}$$

$$D = \beta'_{\alpha_1}\tanh\frac{\mu'_{\alpha_1}}{2}(C_{\alpha_1 1}\Delta Q_1 + C_{\alpha_1 2}\Delta Q_2)^2 + \beta'_{\alpha_2}\tanh\frac{\mu'_{\alpha_2}}{2}(C_{\alpha_2 1}\Delta Q_1 + C_{\alpha_2 2}\Delta Q_2)^2 \quad \text{(A10)}$$

$$A_1 = \beta'_{\alpha_1}\tanh\frac{\mu'_{\alpha_1}}{2}C_{\alpha_1 1}(C_{\alpha_1 1}\Delta Q_1 + C_{\alpha_1 2}\Delta Q_2) + \beta'_{\alpha_2}\tanh\frac{\mu'_{\alpha_2}}{2}C_{\alpha_2 1}(C_{\alpha_2 1}\Delta Q_1 + C_{\alpha_2 2}\Delta Q_2) \quad \text{(A11a)}$$

and

$$A_2 = \beta'_{\alpha_1}\tanh\frac{\mu'_{\alpha_1}}{2}C_{\alpha_1 2}(C_{\alpha_1 1}\Delta Q_1 + C_{\alpha_1 2}\Delta Q_2) + \beta'_{\alpha_2}\tanh\frac{\mu'_{\alpha_2}}{2}C_{\alpha_2 2}(C_{\alpha_2 1}\Delta Q_1 + C_{\alpha_2 2}\Delta Q_2) \quad \text{(A11b)}$$

It follows that

$$G_{12}(t) = K_{12}\sqrt{\frac{\pi^4}{(A_{11}A_{22} - {A_{12}}^2/4)(B_{11}B_{22} - {B_{12}}^2/4)}} \times \exp\left[\frac{{A_1}^2}{4A_{11}} + \frac{\left(A_2 - \frac{A_1A_{12}}{2A_{11}}\right)^2}{4\left(A_{22} - \frac{{A_{12}}^2}{4A_{11}}\right)} - D\right] \quad \text{(A12)}$$

For the three-mixing-mode case, we find

$$G_{123}(t) = K_{123}\sqrt{\frac{\pi^3}{a_{33}(A_{11}A_{22} - {A_{12}}^2/4)}}\sqrt{\frac{\pi^3}{b_{33}(B_{11}B_{22} + {B_{12}}^2/4)}} \times \exp\left[-D + \frac{{A_1}^2}{4A_{11}} + \frac{(A_2 - A_1A_{12}/(2A_{11}))^2}{4(A_{22} - {A_{12}}^2/(4A_{11}))} + \frac{{a_3}^2}{4a_{33}}\right] \quad \text{(A13)}$$

where

$$a_{33} = \left(A_{33} - \frac{{A_{13}}^2}{4A_{11}}\right) - \frac{\left(A_{23} - \frac{A_{12}A_{13}}{2A_{11}}\right)^2}{4\left(A_{22} - \frac{{A_{12}}^2}{4A_{11}}\right)} \quad \text{(A14)}$$

$$a_3 = \left(A_3 - \frac{A_{13}A_1}{2A_{11}}\right) - \frac{\left(A_2 - \frac{A_{12}A_1}{2A_{11}}\right)\left(A_{23} - \frac{A_{12}A_{13}}{2A_{11}}\right)}{2\left(A_{22} - \frac{{A_{12}}^2}{4A_{11}}\right)} \quad \text{(A15)}$$

$$b_{33} = \left(B_{33} - \frac{B_{13}^2}{4B_{11}}\right) - \frac{\left(B_{23} - \frac{B_{12}B_{13}}{2B_{11}}\right)^2}{2\left(B_{22} - \frac{B_{12}^2}{4B_{11}}\right)} \quad \text{(A16)}$$

and

$$K_{123} = \frac{\sqrt{\beta_1\beta_2\beta_3\beta'_{\alpha_1}\beta'_{\alpha_2}\beta'_{\alpha_3}}\sinh\frac{\hbar\omega_1}{2kT}\sinh\frac{\hbar\omega_2}{2kT}\sinh\frac{\hbar\omega_3}{2kT}}{\sqrt{2^6\pi^6\sinh\lambda_1\sinh\lambda_2\sinh\lambda_3\sinh\mu'_{\alpha_1}\sinh\mu'_{\alpha_2}\sinh\mu'_{\alpha_3}}} \quad \text{(A17)}$$

Similarly, for the four mixing-mode case, we have

$$G_{1234}(t) = K_{1234}\sqrt{\frac{\pi^4}{\left(A_{11}A_{22} - \frac{A_{12}^2}{4}\right)\left(a_{33}a_{44} - \frac{a_{34}^2}{4}\right)}} \times \sqrt{\frac{\pi^4}{\left(B_{11}B_{22} - \frac{B_{12}^2}{4}\right)\left(b_{33}b_{44} - \frac{b_{34}^2}{4}\right)}}\exp\left[-D + \frac{A_1^2}{4A_{11}} + \frac{\left(A_2 - \frac{A_{12}A_1}{2A_{11}}\right)^2}{4\left(A_{22} - \frac{A_{12}^2}{4A_{11}}\right)} + \frac{a_3^2}{4a_{33}} + \frac{\left(a_4 - \frac{a_{34}a_3}{2a_{33}}\right)^2}{4\left(a_{44} - \frac{a_{34}^2}{4a_{33}}\right)}\right] \quad \text{(A18)}$$

where

$$a_{44} = \left(A_{44} - \frac{A_{14}^2}{4A_{11}}\right) - \frac{\left(A_{24} - \frac{A_{12}A_{14}}{2A_{11}}\right)^2}{4(A_{22} - A_{12}^2/4A_{11})} \quad \text{(A19)}$$

$$a_4 = \left(A_4 - \frac{A_{14}A_1}{2A_{11}}\right) - \frac{\left(A_2 - \frac{A_{12}A_1}{2A_{11}}\right)\left(A_{24} - \frac{A_{12}A_{14}}{2A_{11}}\right)}{2(A_{22} - A_{12}^2/(4A_{11}))} \quad \text{(A20)}$$

$$a_{34} = \left(A_{34} - \frac{A_{13}A_{14}}{2A_{11}}\right) - \frac{\left(A_{23} - \frac{A_{12}A_{13}}{2A_{11}}\right)\left(A_{24} - \frac{A_{12}A_{14}}{2A_{11}}\right)}{2\left(A_{22} - \frac{A_{12}^2}{4A_{11}}\right)} \quad \text{(A21)}$$

$$b_{34} = \left(B_{34} - \frac{B_{13}B_{14}}{2B_{11}}\right) - \frac{\left(B_{23} - \frac{B_{12}B_{13}}{2B_{11}}\right)\left(B_{24} - \frac{B_{12}B_{14}}{2B_{11}}\right)}{2\left(B_{22} - \frac{B_{12}^2}{4B_{11}}\right)} \quad \text{(A22)}$$

$$b_{44} = \left(B_{44} - \frac{B_{14}^2}{4B_{11}}\right) - \frac{\left(B_{24} - \frac{B_{12}B_{14}}{2B_{11}}\right)^2}{4\left(B_{22} - \frac{B_{12}^2}{4B_{11}}\right)} \quad \text{(A23)}$$

and

$$K_{1234} = \frac{\sqrt{\beta_1\beta_2\beta_3\beta_4\beta'_{\alpha_1}\beta'_{\alpha_2}\beta'_{\alpha_3}\beta'_{\alpha_4}}\sinh\frac{\hbar\omega_1}{2kT}\sinh\frac{\hbar\omega_2}{2kT}\sinh\frac{\hbar\omega_3}{2kT}\sinh\frac{\hbar\omega_4}{2kT}}{\sqrt{2^8\pi^8\sinh\lambda_1\sinh\lambda_2\sinh\lambda_3\sinh\lambda_4\sinh\mu'_{\alpha_1}\sinh\mu'_{\alpha_2}\sinh\mu'_{\alpha_3}\sinh\mu'_{\alpha_4}}} \quad \text{(A24)}$$

Appendix B

In this appendix, we shall briefly derive an alternative expression of eq A12 convenient for the numerical computation. By defining

$$g_{\pm}(n'_{j\alpha}) = (1 + n'_{j\alpha})\,e^{-\mu'_\alpha} \pm n'_{j\alpha}\,e^{\mu'_\alpha} \quad \text{(B1)}$$

and

$$n'_{j\alpha} = \frac{1}{e^{\lambda_j + \mu'_\alpha} - 1} \quad \text{(B2)}$$

we find[99]

$$G_{12}(t) = 2^2\sqrt{\beta_1\beta_2\beta'_{\alpha_1}\beta'_{\alpha_2}}n'_{1\alpha_1}n'_{2\alpha_2}(e^{\hbar\omega_1/(kT)} - 1)(e^{\hbar\omega_2/(kT)} - 1)\frac{\exp[it(\omega_1 + \omega_2 - \omega_{\alpha_1} - \omega_{\alpha_2})/2]}{\sqrt{F_-^{\mathrm{mix}}F_+^{\mathrm{mix}}}}\exp\left[-\frac{g_{\mathrm{mix}}}{F_+^{\mathrm{mix}}}\right] \quad \text{(B3)}$$

where

$$g_{\mathrm{mix}} = \beta_1\beta'_{\alpha_1}\left[\beta_2\Delta Q_{\alpha_1}^2\{1 + g_-(n'_{2\alpha_2})\} + \beta'_{\alpha_2}\begin{vmatrix}\Delta Q_{\alpha_1} & C_{\alpha_1 2}\\ \Delta Q_{\alpha_2} & C_{\alpha_2 2}\end{vmatrix}^2\{1 - g_-(n'_{2\alpha_2})\}\right]g_{\mathrm{disp}}(n'_{1\alpha_1}) + \beta_2\beta'_{\alpha_2}\left[\beta_1\Delta Q_{\alpha_2}^2\{1 + g_-(n'_{1\alpha_1})\} + \beta'_{\alpha_1}\begin{vmatrix}C_{\alpha_1 1} & \Delta Q_{\alpha_1}\\ C_{\alpha_2 1} & \Delta Q_{\alpha_2}\end{vmatrix}^2\{1 - g_-(n_{1\alpha_1})\}\right]g_{\mathrm{disp}}(n'_{2\alpha_2}) \quad \text{(B4)}$$

$$g_{\mathrm{disp}}(n'_{j\alpha}) = 1 + 2n'_{j\alpha} - g_+(n'_{j\alpha}) \quad \text{(B5)}$$

$$F_+^{\mathrm{mix}} = [\beta_1\beta_2\{1 + g_-(n'_{1\alpha_1})\}\{1 + g_-(n'_{2\alpha_2})\} + \beta'_{\alpha_1}\beta'_{\alpha_2}(C_{\alpha_1 2}C_{\alpha_2 1} - C_{\alpha_1 1}C_{\alpha_2 2})^2\{1 - g_-(n'_{1\alpha_1})\}\{1 - g_-(n'_{2\alpha_2})\} + \beta_1\beta'_{\alpha_2}(C_{\alpha_2 2})^2\{1 + g_-(n'_{1\alpha_1})\}\{1 - g_-(n'_{2\alpha_2})\} + \beta_2\beta'_{\alpha_1}(C_{\alpha_1 1})^2\{1 - g_-(n'_{1\alpha_1})\}\{1 + g_-(n'_{2\alpha_2})\} + \{(1 + n'_{1\alpha_1})\exp[-(\mu_{\alpha_1} - \mu_{\alpha_2})] - n'_{1\alpha_1}\}\{(1 + n'_{2\alpha_2})\exp(\mu_{\alpha_1} - \mu_{\alpha_2}) - n'_{2\alpha_2}\}[\beta_1\beta'_{\alpha_1}(C_{\alpha_1 2})^2\{1 + g_-(n'_{1\alpha_2})\}\{1 - g_-(n'_{2\alpha_1})\} + \beta_2\beta'_{\alpha_2}(C_{\alpha_2 1})^2\{1 - g_-(n'_{1\alpha_2})\}\{1 + g_-(n'_{2\alpha_1})\}]] \quad \text{(B6)}$$

and

$$F_{-}^{\mathrm{mix}} = [\beta_1\beta_2\{1 - g_{-}(n'_{1\alpha_1})\}\{1 - g_{-}(n'_{2\alpha_2})\} + \beta'_{\alpha_1}\beta'_{\alpha_2} (C_{\alpha_1 2}C_{\alpha_2 1} - C_{\alpha_1 1}C_{\alpha_2 2})^2\{1 + g_{-}(n'_{1\alpha_1})\}\{1 + g_{-}(n'_{2\alpha_2})\} + \beta_1\beta'_{\alpha_2}(C_{\alpha_2 2})^2\{1 - g_{-}(n'_{1\alpha_1})\}\{1 + g_{-}(n'_{2\alpha_2})\} + \beta_2\beta'_{\alpha_1}(C_{\alpha_1 1})^2 \{1 + g_{-}(n'_{1\alpha_1})\}\{1 - g_{-}(n'_{2\alpha_2})\} + \{(1 + n'_{1\alpha_1})\exp[-(\mu'_{\alpha_1} - \mu'_{\alpha_2})] - n'_{1\alpha_1}\}\{(1 + n'_{2\alpha_2})\exp(\mu'_{\alpha_1} - \mu'_{\alpha_2}) - n'_{2\alpha_2}\}[\beta_1\beta'_{\alpha_1} (C_{\alpha_1 2})^2\{1 - g_{-}(n'_{1\alpha_2})\}\{1 + g_{-}(n'_{2\alpha_1})\} + \beta_2\beta'_{\alpha_2}(C_{\alpha_2 1})^2\{1 + g_{-}(n'_{1\alpha_2})\}\{1 - g_{-}(n'_{2\alpha_1})\}]] \quad \text{(B7)}$$

Appendix C

In this appendix, we shall show an alternative expression of eq 16 convenient for the numerical computation. Applying eqs B1, B2, and B5 to eq 16 leads to[99]

$$G_l(t) = \frac{2\sqrt{\beta_l\beta'_l}}{\beta_l + \beta'_l} n'_l(e^{\hbar\omega_l/(kT)} - 1)\frac{e^{it(\omega_l - \omega'_l)/2}}{\sqrt{f_+ f_-}} \exp\left[-\frac{\beta_l\beta'_l(\Delta Q_l)^2}{(\beta_l + \beta'_l)}\frac{g_{\mathrm{disp}}(n'_l)}{f_+}\right] \quad \text{(C1)}$$

where

$$f_{\pm} = \left\{1 \pm \frac{\beta_l - \beta'_l}{\beta_l + \beta'_l} g_{-}(n'_l)\right\} \quad \text{(C2)}$$

and

$$n'_l = \frac{1}{e^{\lambda_l + \mu'_l} - 1} = \frac{1}{e^{it(\omega_l - \omega'_l) + \hbar\omega_l/(kT)} - 1} \quad \text{(C3)}$$

From eq C1, it is easy to see two simple cases, i.e., the displaced harmonic potential surface case $\beta_l = \beta'_l$ and $\Delta Q_l \neq 0$ and the distorted harmonic potential surface case $\beta_l \neq \beta'_l$ and $\Delta Q_l = 0$. For the displaced and distorted harmonic potential surface cases, the correlation functions $G_l(t)$ become

$$G_l(t) = \exp[-S_l\, g_{\mathrm{disp}}(n_l)] \quad \text{(C4)}$$

and

$$G_l(t) = \frac{2\sqrt{\beta_l\beta'_l}}{\beta_l + \beta'_l} n'_l(e^{\hbar\omega_l/(kT)} - 1)\frac{e^{it(\omega_l - \omega'_l)/2}}{\sqrt{f_+ f_-}} \quad \text{(C5)}$$

respectively. Here, in eq C4, $S_l = \beta_l(\Delta Q_l)^2/2$ denotes the Huang−Rhys factor and

$$n_l = \frac{1}{e^{\hbar\omega_l/(kT)} - 1}$$

Appendix D

In this appendix, we shall obtain an alternative expression of eq 21 convenient for the numerical computation. Applying eqs B1, B2, and C2 to eq 21 yields[99]

$$K_{\mathrm{p}}(t) = G_{\mathrm{p}}(t) \left[\frac{\omega_l\omega'_l}{\hbar(\omega_l + \omega'_l)}\frac{\left\{g_{+}(n'_l) + \frac{(\omega_l - \omega'_l)}{(\omega_l + \omega'_l)} g_{-}(n'_l)(1 + 2n'_l)\right\}}{f_+ f_-} + \frac{\omega_l\omega'_l}{\hbar(\omega_l + \omega'_l)}\frac{\omega_l\omega'_l(\Delta Q_l)^2}{\hbar(\omega_l + \omega'_l)}\frac{[1 + 2n'_l - g_{+}(n'_l)]^2}{f_+ f_+}\right] \quad \text{(D1)}$$

where $g_{-}(n'_l)$ and $g_{+}(n'_l)$ are given by eq B1 and f_+ and f_- are given by eq C2. In the case in which the promoting mode is not displaced−distorted, eq D1 becomes

$$K_{\mathrm{p}}(t) = \frac{\omega_l}{2\hbar} G_{\mathrm{p}}(t)\, g_{+}(n_l) = \frac{\omega_l}{2\hbar} G_{\mathrm{p}}(t)\, \{(1 + n_l)\, e^{-\mu_\alpha} + n_l\, e^{\mu_\alpha}\} \quad \text{(D2)}$$

In the low-temperature limit, i.e., $\hbar\omega_l \gg kT$ or $n'_l = 0$, we have

$$K_{\mathrm{p}}(t) = \frac{\omega_l}{2\hbar} G_{\mathrm{p}}(t)\, e^{it\omega_l} \quad \text{(D3)}$$

References and Notes

(1) Mebel, A. M.; Hayashi, M.; Lin S. H. In *Trends in Physical Chemistry*; Research Trends: India, 1997; p 315.
(2) (a) Schlegel, H. B.; Robb, M. A. *Chem. Phys. Lett.* **1982**, *93*, 43. (b) Bernardi, F.; Bottoni, A.; McDougall, J. J. W.; Robb, M. A.; Schlegel, H. B. *Faraday Symp. Chem. Soc.* **1984**, *19*, 137. (c) Werner, H.-J.; Knowles, P. J. *J. Chem. Phys.* **1985**, *82*, 5053. (d) Knowles, P. J.; Werner, H.-J. *Chem. Phys. Lett.* **1985**, *115*, 259.
(3) Stanton, J. F.; Bartlett, R. J. *J. Chem. Phys.* **1993**, *98*, 7029.
(4) (a) Werner, H.-J.; Knowles, P. J. *J. Chem. Phys.* **1988**, *89*, 5803. (b) Knowles, P. J.; Werner, H.-J. *Chem. Phys. Lett.* **1988**, *145*, 514.
(5) (a) Andersson, K.; Malmqvist, P.-Å.; Roos, B. O.; Sadlej, A. J.; Wolinsky, K. *J. Phys. Chem.* **1990**, *94*, 5483. (b) Andersson, K.; Malmqvist, P.-Å.; Roos, B. O. *J. Chem. Phys.* **1992**, *96*, 1218. (c) Werner, H.-J. *Mol. Phys.* **1996**, *89*, 645.
(6) Duschinsky, F. *Acta Physicochim. (USSR)* **1937**, *7*, 551.
(7) Wunsch, L.; Metz, F.; Neusser, H. J.; Schlag, E. W. *J. Chem. Phys.* **1977**, *66*, 386.
(8) Small, G. J. *J. Chem. Phys.* **1971**, *54*, 3300.
(9) Warren, J. A.; Hayes, J. M.; Small, G. J. *J. Chem. Phys.* **1984**, *80*, 1786.
(10) Mochizuchi, Y.; Kaya, K.; Ito, M. *Chem. Phys.* **1981**, *54*, 375.
(11) Lacey, A. R.; McCoy, E. F.; Ross, I. G. *Chem. Phys. Lett.* **1973**, *21*, 233.
(12) Burke, F. B.; Eslinger, D. R.; Small, G. J. *J. Chem. Phys.* **1975**, *63*, 1309.
(13) Small, G. J.; Burke, F. B. *J. Chem. Phys.* **1977**, *66*, 1767.
(14) Hemley, R. J.; Leopold, D. G.; Vaida, V.; Karplus, M. *J. Chem. Phys.* **1985**, *82*, 5379.
(15) Eiden, G. C.; Weisshaar, J. C. *J. Chem. Phys.* **1996**, *104*, 8896.
(16) Lunardi, G.; Pecile, C. *J. Chem. Phys.* **1991**, *95*, 6911.
(17) Falchi, A.; Gellini, C.; Salvi, P. R.; Hafner, K. *J. Phys. Chem.* **1995**, *99*, 14659.
(18) Sinclair, W. E.; Yu, H.; Phillips, D. *J. Chem. Phys.* **1997**, *106*, 5797.
(19) Swinn, A. K.; Kable, S. H. *J. Mol. Spectrosc.* **1998**, *191*, 49.
(20) Singh, K. M.; Singh, R. A.; Thakur, S. N. *Indian J. Pure Appl. Phys.* **1997**, *35*, 5.
(21) Burova, T. G. *Opt. Spektrosk.* **1994**, *76*, 394.
(22) Zborowski, K.; Pawlikowski, M. *Acta Phys. Pol. A* **1995**, *88*, 435.
(23) Hohlneicher, G.; Wolf, J. *Phys. Status Solidi B* **1995**, *189*, 59.
(24) Book, L. D.; Arnett, D. C.; Hu, H.; Scherer, N. F. *J. Phys. Chem. A* **1998**, *102*, 4350.
(25) Troxler, T. *J. Phys. Chem. A* **1998**, *102*, 4775.
(26) Hong, H.-K. *J. Chem. Phys.* **1978**, *68*, 1253.
(27) Mukamel, S.; Loring, S. F. *J. Opt. Soc. Am.* **1986**, *B3*, 595.
(28) Deng, Z. F.; Mukamel, S. *J. Chem. Phys.* **1986**, *85*, 1738.
(29) Vallet, J. C.; Boeglin, A. J.; Lavoine, J. P.; Villaeys, A. A. *J. Chin. Chem. Soc.* **1995**, *42*, 195.
(30) Hayashi, M.; Mebel, A. M.; Liang, K. K.; Lin, S. H. *J. Chem. Phys.* **1998**, *108*, 2044.

(31) Peluso, A.; Santoro, F.; Del Re, G. *Int. J. Quantum Chem.* **1997**, *63*, 233.
(32) Held, A.; Champagne, B. B.; Pratt, D. W. *J. Chem. Phys.* **1991**, *95*, 8732.
(33) Gavin, R. M., Jr.; Risemberg, S.; Rice, S. A. *J. Chem. Phys.* **1973**, *58*, 3100.
(34) Leopold, D. G.; Pendley, R. D.; Roebber, J. L.; Hemley, R. J.; Vaida, V. *J. Chem. Phys.* **1984**, *81*, 4218.
(35) Petelenz, P.; Petelenz, B. *J. Chem. Phys.* **1975**, *62*, 3482.
(36) Hemley, R. J.; Lasaga, A. C.; Vaida, V.; Karplus, M. *J. Phys. Chem.* **1988**, *92*, 945.
(37) Zerbetto, F.; Zgierski, M. *J. Chem. Phys.* **1993**, *98*, 4822.
(38) Coon, J. B.; DeWames, R. E.; Loyd, C. M. *J. Mol. Spectrosc.* **1962**, *8*, 285.
(39) Atabek, O.; Bourgeois, M. T.; Jacon, M. *J. Chem. Phys.* **1987**, *87*, 5870.
(40) Atabek, O.; Bourgeois, M. T.; Jacon, M. *J. Chem. Phys.* **1986**, *84*, 6699.
(41) (a) Smith, W. L. *J. Mol. Spectrosc.* **1996**, *176*, 95. (b) Smith, W. L. *J. Mol. Spectrosc.* **1998**, *187*, 6.
(42) Sharp, T. E.; Rosenstock, H. M. *J. Chem. Phys.* **1964**, *41*, 3453.
(43) Smith, W. L.; Warsop, P. A. *Trans. Faraday Soc.* **1968**, *64*, 1165.
(44) Hutchisson, E. *Phys. Rev.* **1930**, *36*, 410.
(45) Warshel, A.; Karplus, M. *Chem. Phys. Lett.* **1972**, *17*, 7.
(46) Warshel, A. *J. Chem. Phys.* **1975**, *62*, 214.
(47) Doktorov, E. V.; Malkin, I. A.; Man'ko, V. I. *J. Mol. Spectrosc.* **1975**, *56*, 21.
(48) Doktorov, E. V.; Malkin, I. A.; Man'ko, V. I. *J. Mol. Spectrosc.* **1977**, *64*, 302.
(49) Kupka, H.; Cribb, P. H. *J. Chem. Phys.* **1986**, *85*, 1303.
(50) Faulkner, T. R.; Richardson, F. S. *J. Chem. Phys.* **1979**, *70*, 1201.
(51) Subbi, J. *Chem. Phys.* **1988**, *122*, 157.
(52) Ozkan, I. *Int. J. Quantum Chem.* **1984**, *25*, 339.
(53) Chen, K. M.; Pei, C. C. *Chem. Phys. Lett.* **1990**, *165*, 523.
(54) Baranov, V. I.; Zelentsov, D. Yu. *Zh. Strukt. Khim.* **1995**, *36*, 217.
(55) Zerbetto, F.; Zgierski, M. Z. *Chem. Phys.* **1988**, *127*, 17.
(56) Zerbetto, F.; Zgierski, M. Z. *Chem. Phys. Lett.* **1988**, *144*, 437.
(57) Zerbetto, F.; Zgierski, M. Z. *Chem. Phys. Lett.* **1989**, *157*, 515.
(58) Venuti, E.; Marconi, G. *J. Mol. Struct.* **1992**, *266*, 235.
(59) Chau, F.-T.; Lee, E. P.-F.; Wang, D.-C. *J. Phys. Chem. A* **1997**, *101*, 1603.
(60) Chen, P. Photoelectron Spectroscopy of Reactive Intermediates. In *Unimolecular and Bimolecular Reaction Dynamics*; Ng, C. Y., Baer, M., Powis, I., Eds.; John Wiley and Sons: New York, 1994.
(61) Crane, J. C.; Nam, H.; Beal, H. P.; Clauberg, H.; Choi, Y. S.; Moore, C. B.; Stanton, J. F. *J. Mol. Spectrosc.* **1997**, *181*, 56.
(62) Clauberg, H.; Chen, P. *J. Phys. Chem.* **1992**, *96*, 5676.
(63) Mebel, A. M.; Chen, Y.-T.; Lin, S. H. *Chem. Phys. Lett.* **1996**, *258*, 53.
(64) Mebel, A. M.; Chen, Y.-T.; Lin, S. H. *J. Chem. Phys.* **1996**, *105*, 9007.
(65) Mebel, A. M.; Lin, S. H.; Chang, C.-H. *J. Chem. Phys.* **1997**, *106*, 2612.
(66) Mebel, A. M.; Lin, S. H. *Chem. Phys.* **1997**, *215*, 329.
(67) Mebel, A. M.; Chen, Y.-T.; Lin, S. H. *Chem. Phys. Lett.* **1997**, *275*, 19.
(68) Jackson, W. M.; Mebel, A. M.; Lin, S. H.; Lee, Y. T. *J. Phys. Chem. A* **1997**, *101*, 6638.
(69) Mebel, A. M.; Jackson, W. M.; Chang, A. H. H.; Lin, S. H. *J. Am. Chem. Soc.* **1998**, *120*, 5751.
(70) Liao, D. W.; Mebel, A. M.; Hayashi, M.; Shiu, Y. J.; Chen, Y.-T.; Lin, S. H. *J. Chem. Phys.* **1999**, *111*, 205.
(71) Lin, S. H. *Proc. R. Soc. London* **1976**, *A352*, 57.
(72) Lin, S. H. *J. Chem. Phys.* **1966**, *44*, 3759.
(73) Lin, S. H.; Bersohn, R. *J. Chem. Phys.* **1968**, *48*, 2732.
(74) Lin, S. H. *J. Chem. Phys.* **1973**, *58*, 5760.
(75) Islampour, R.; Dehestani, M.; Lin, S. H. *J. Mol. Spectrosc.* **1999**, *194*, 179.
(76) Robin, M. B. *Higher Excited States of Polyatomic Molecules*; Academic Press: New York, 1975; Vol. 2, p 2; Vol. 3, p 213.
(77) (a) Wilkinson, P. G.; Mulliken, R. S. *J. Chem. Phys.* **1955**, *23*, 1895. (b) Wilkinson, P. G. *J. Mol. Spectrosc.* **1961**, *6*, 1.
(78) Foo, P. D.; Innes, K. K. *J. Chem. Phys.* **1974**, *60*, 4582.
(79) Petrongolo, C.; Buenker, R. J.; Peyerimhoff, S. D. *J. Chem. Phys.* **1982**, *76*, 3655; **1983**, *78*, 7284.
(80) Nakatsuji, H. *J. Chem. Phys.* **1984**, *80*, 3703.
(81) Palmer, M. H.; Beveridge, A. J.; Walker, I. C.; Abuain, T. *Chem. Phys.* **1986**, *102*, 63.
(82) Siebrand, W.; Zerbetto, F.; Zgiersky, M. *Chem. Phys. Lett.* **1990**, *174*, 119.
(83) Foresman, J. B.; Head-Gordon, M.; Pople, J. A.; Frisch, M. J. *J. Phys. Chem.* **1992**, *96*, 135.
(84) Wiberg, K. B.; Hadad, C. M.; Foresman, J. B.; Chupka, W. A. *J. Phys. Chem.* **1992**, *96*, 10756.
(85) Serrano-Andres, L.; Merchan, M.; Nebot-Gil, I.; Lindh, R.; Roos, B. O. *J. Chem. Phys.* **1993**, *98*, 3151.
(86) Lindh, R.; Roos, B. O. *Int. J. Quantum Chem.* **1989**, *35*, 813.
(87) Ryu, J.-S.; Hudson, B. S. *Chem. Phys. Lett.* **1995**, *245*, 448.
(88) Fuke, K.; Schnepp, O. *Chem. Phys.* **1979**, *38*, 211.
(89) Rabalais, J. W.; McDonald, J. M.; Scherr, V.; McGlynn, S. P. *Chem. Rev.* **1971**, *71*, 73.
(90) Iverson, A. A.; Russell, B. R. *Spectrochim. Acta, Part A* **1972**, *28*, 447.
(91) Chen, Y. T. Private communications.
(92) Buenker, R. J.; Peyerimhoff, S. D. *Chem. Rev.* **1974**, *74*, 127.
(93) (a) Becke, A. D. *J. Chem. Phys.* **1993**, *98*, 5648. (b) Becke, A. D. **1992**, *96*, 2155. (c) Becke, A. D. **1992**, *97*, 9173.
(94) Lee, C.; Yang, W.; Parr, R. G. *Phys. Rev.* **1988**, *B37*, 785.
(95) Martin, P. S.; Yates, K.; Csizmadia, I. G. *J. Mol. Struct.: THEOCHEM* **1988**, *170*, 107.
(96) Lam, B.; Johnson, R. P. *J. Am. Chem. Soc.* **1983**, *105*, 7479.
(97) Bettinger, H. F.; Schreiner, P. R.; Schleyer, P. v. R.; Schaefer, H. F., III. *J. Phys. Chem.* **1996**, *100*, 16147.
(98) Scott, A. P.; Radom, L. *J. Phys. Chem.* **1996**, *100*, 16502.
(99) Hayashi, M.; Liang, K. K.; Mebel, A. M.; Lin, S. H. Manuscript in preparation.